Photino Hypothesis III: Field-Theoretic Reconstruction of Magnetism and a Unified Phenomenological Mechanism

Tuanhua Chen
(Independent Researcher, Guilin, China 541000)
Corresponding author: Tuanhua Chen E-mail: 574581920@qq.com

Abstract

The physical origin of magnetic interaction and its inherent unification with macroscopic quantum phenomena, such as superconductivity and superfluidity, represent two long-separated core challenges in modern physics. As the third paper in the “Photino Hypothesis” series, this work proposes a unified framework based on the spacetime photino background established in preceding studies: **the essence of magnetism is a local photino vortex excited by spinning particles, while superconductivity and superfluidity are the quantum coherent states in which this vortex field is globally suppressed or ordered at the macroscopic scale**. This work constructs three theoretical pillars: (1) The **Spin-Vortex Field Mode**l, which interprets spin angular momentum as the source driving the photino medium to produce directed circulation, with the magnetic induction **B** being the curl of this flow; (2) The **Vortex Field Explanation of Flux Quantization**, attributing the flux quantum in superconductors to the circulation quantization condition of the photino vortex ring; (3) The **Order Parameter Unification of Macroscopic Quantum States**, indicating that the macroscopic coherence in superconductors and superfluids originates from the phase stiffness provided by the photino background field. This theory provides, for the first time, a coherent explanation based on the same medium dynamics for key phenomena including the origin of magnetic fields, the zero-resistance and Meissner effects in superconductors, and the non-viscosity and vortex lattice in superfluids. Furthermore, the theory unifies classic magneto-optical phenomena such as the Faraday effect, Kerr effect, and Zeeman effect under the picture of **Coulomb interaction between the photino flow and photons**, and proposes novel, testable predictions like the magnetically induced anisotropy of the speed of light. This work aims to return the description of electromagnetic interaction from abstract field theory to the dynamics of a real medium, opening a new paradigm for the unified understanding of electromagnetic effects and macroscopic quantum phenomena.

Keywords: Photino; Nature of Magnetic Field; Superconductor; Superfluid; Magneto-optical Effect; Electron Spin Resonance

1. Introduction

Magnetic phenomena, serving as the core carrier of electromagnetic interactions, represent a critical aspect in the construction of a unified physical theory. From Oersted's discovery of the magnetic effect of electric currents and Ampère's molecular current hypothesis [3], to Maxwell's establishment of a unified theory of electromagnetic fields [4], the phenomenological description of macroscopic magnetic phenomena has been thoroughly developed. However, the fundamental question regarding the microscopic dynamical mechanism of magnetic field generation remains unresolved: while Maxwell's equations perfectly describe the macroscopic behavior of

electromagnetic fields, they fail to reveal the microscopic picture of field-matter interaction; quantum electrodynamics describes magnetic interactions through virtual photon exchange [5], yet still faces conceptual and computational challenges when explaining specific phenomena such as superconducting diamagnetism and magneto-optical effects.

Magnetism and superconductivity-superfluidity represent two extreme physical worlds, spanning from microscopic spin to macroscopic quantum coherence. Although Maxwell's equations and the Ginzburg-Landau theory have achieved great success in their respective domains, a profound connection at the physical origin between them remains lacking: the physical entity of magnetic induction **B** remains obscure, while the Cooper pairs in superconductors and Bose-Einstein condensation in superfluids, though mathematically elegant, lack a clarified medium background for their interactions.

The core dilemma of current theories can be summarized as a "dichotomous separation":

(1) **Separation between the microscopic and macroscopic:** The microscopic origin of magnetism (spin magnetic moment) and its macroscopic manifestation (magnetic field) are connected through statistical averaging, lacking a medium-based picture that continuously transitions from microscopic particle dynamics to macroscopic fields.

(2) **Separation between electromagnetic and macroscopic quantum phenomena**: Theories of superconductivity and superfluidity are built upon phenomenological order parameters and gauge symmetry breaking, failing to achieve unification with the microscopic carrier of electromagnetic fields at the physical mechanism level.

In the first two papers of this series, we established the theoretical foundation of the "Photino Hypothesis": spacetime consists of a continuous medium of negatively charged photinos, whose distribution gradient $\nabla\sigma_p$ manifests as gravity, and the gravitational constant is deconstructed as $G = R_m \cdot k_e \cdot Q_{m0}^2$, achieving a preliminary unification of gravity and electromagnetic forces at the microscopic mechanism level for the first time [1, 2]. This paper aims to extend this theoretical framework into the realms of magnetism and macroscopic quantum phenomena, proposing a core thesis: **magnetism is the vortex motion mode of the photino medium, while superconductivity and superfluidity are the direct results of this vortex mode being globally constrained or ordered when the medium enters a macroscopic quantum coherent state.**

This theory is built upon the following three innovative pillars:

1. Spin as the Vortex Source: The Medium Picture of Magnetism

The intrinsic spin of electrons and other fermions, through interaction with the photino medium [1,2], drives it to generate directional circulation around the spin axis, forming a stable microscopic vortex structure. The curl of this vortex is observed as the magnetic induction **B.** This fundamentally elevates magnetism from "an effect of moving charges" to "a medium vortex field induced by spin."

2. Quantization and Suppression of the Vortex Field: The Essence of Superconductivity and Superfluidity

In the superconducting state, the coherent condensation of Cooper pairs forces the photino

vortex field to be completely expelled from the bulk (Meissner effect), existing only in the form of quantized vortex lines within the flux lattice of type-II superconductors, whose quantization condition shares the same origin as the circulation properties of the photino vortex field. In the superfluid state, the Bose condensate allows quantized vortices to exist as elementary excitations.

3. Unified Origin of the Order Parameter: Phase Stiffness from the Medium Background

The macroscopic quantum phase coherence in superconductivity and superfluidity originates from the non-zero phase stiffness provided by the photino background field. This unifies electromagnetic gauge symmetry and macroscopic quantum phase symmetry at the medium level.

This paper will systematically elaborate on how the photino vortex field theory uniformly explains magnetic, superconducting, and superfluid phenomena, and will provide testable experimental predictions, aiming to open a new pathway based on real medium dynamics for understanding these core physical phenomena.

2 Field-Theoretic Reconstruction of the Nature of Magnetism and Medium Dynamics

Based on the framework of the unified photino field theory, and integrating the microscopic origin of gravity established in **Hypothesis I** [1] and the field theory of light constructed in **Hypothesis II** [2], this section aims to provide a microscopic explanation for magnetic phenomena based on medium dynamics. We propose that the essence of the magnetic field is a flow field effect generated by the coupling between electron motion and photino dynamics. By unifying the parameter systems of the three hypotheses, this theory achieves self-consistency while also revealing a deeper level of unity between electromagnetic and gravitational interactions.

2.1 The Essence of the Magnetic Field: The Dynamic Model of Photino Flow

2.1.1 Microscopic Mechanism of the Magnetic Field

The physical essence of the magnetic field obtains a complete and coherent dynamical picture within this theory (as shown in Figure 2.1): **the magnetic field is a dynamic flow field formed by moving electrons driving photinos through quantum coupling**. According to the fundamental differences in the physical nature of the excitation mechanisms, magnetic fields can be classified into two basic forms:

- **Sourceless Magnetic Field**: Formed by the **coordinated driving of the spin and translational velocity of moving electrons** on photinos, resulting in a **non-closed helical circulation**. This form corresponds to the sourceless field property in Maxwell's equations, $\nabla \cdot \vec{B} = 0$.
- **Source Magnetic Field**: Formed by a **time-varying electric field** accelerating photinos via the

Coulomb force, resulting in an **irrotational transient directional flow field**. This form corresponds to the source field property in Maxwell's equations, $\nabla \times \vec{B} = \mu_0 \vec{J} + \mu_0 \varepsilon_0 \frac{\partial \vec{E}}{\partial t}$.

This classification not only directly corresponds to the mathematical structure of Maxwell's equations but also achieves a fundamental reconstruction of the physical picture. Unlike traditional models of electron spin magnetic moment and orbital magnetic moment [10], this theory thoroughly reduces magnetic phenomena to the more fundamental dynamical processes of the photino medium, thereby establishing a complete descriptive framework from microscopic mechanisms to macroscopic phenomena.

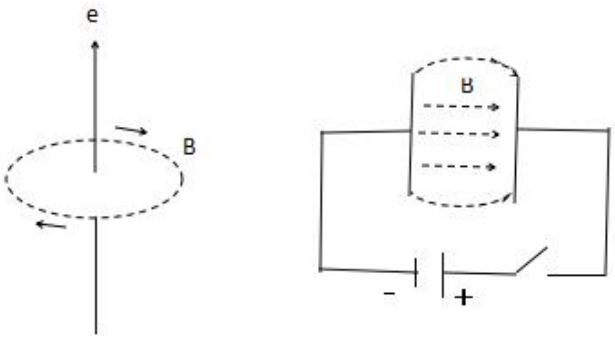

Fig. 2.1

2.1.2 Sourceless Magnetic Field: Photino Helical Circulation Driven by Electron Motion and the Parameter System

This section is based on the theoretical framework of Photino Hypothesis III, integrating the microscopic origin of gravity from **Hypothesis I** and the field theory of light from **Hypothesis II**, to establish a microscopic circulation model for the sourceless magnetic field. By unifying the parameter systems of the three hypotheses to achieve theoretical self-consistency, the "magnetic field" is thus reduced to the dynamical outcome of the interaction between moving electrons and the photino medium.

Core Physical Mechanism

1. Coordinated Driving Mechanism of Electron Motion and Spin

The spin angular momentum $\vec{S} = \sqrt{s(s+1)}h \cdot \hat{S} = \frac{\sqrt{3}}{2}h \cdot \hat{S}$ of an isolated, stationary electron $(\vec{v}_e = 0)$ is insufficient to excite sustained directional circulation in the photino medium. The key lies in the electron being in a state of motion （$\vec{v}_e \neq 0$） . Its velocity and spin angular momentum produce a synergistic effect:

- **Spin Component:** Drives photinos to undergo rotational motion around the electron's spin axis direction $\hat{S}$.
- **Motion Component**: Drags these rotating photinos, producing translation along the electron's direction of motion $\vec{v}_e$.

The synergistic action of these two components "stretches" the photino's trajectory from a closed circular loop around the spin axis into a **non-closed helix** with an axial translational component, forming the microscopic dynamical basis for magnetic field generation.

2. Quantized Derivation of the Photino Velocity Field

A single electron, through quantum coupling, strongly interacts with a fixed number n_p of photinos. Each photino receives a portion of the electron's total spin angular momentum. According to angular momentum conservation and quantization conditions, the angular momentum acquired by a single photino is:

$$\boldsymbol{L_p = \frac{S}{n_p} = \frac{\sqrt{3}\hbar}{2n_p}} \qquad \textbf{(2.1)}$$

Using the classical angular momentum relation $L_p = m_p v_{p,spin} r_e$, the photino rotational angular velocity induced by the spin component can be solved:

$$\boldsymbol{\vec{\omega} = \frac{\vec{v}_{p,spin}}{r} = \frac{\sqrt{3}\hbar}{2n_p m_p {r_e}^2}\left(\hat{S} \times \hat{r}\right)} \qquad \textbf{(2.2)}$$

Superposing the drag velocity from the electron's translation, $\vec{v}_{p,trans} = \vec{v}_e$, yields the microscopic expression for the total photino velocity field:

$$\vec{v}_p(\vec{r}) = \underbrace{\frac{\sqrt{3}\hbar}{2n_p m_p {r_e}^2}\left(\hat{S} \times \hat{r}\right)}_{\textbf{Spin Circulation Component}} + \underbrace{\vec{v}_e}_{\textbf{Motion Drag Component}} \qquad \textbf{(2.3)}$$

Physical Meaning: This equation indicates that the photino flow corresponding to the magnetic field is a superposition of rotation and translation. The motion drag component plays a key role in explaining phenomena such as the **magneto-optical effect**.

3. Dynamical Foundation of Photino Circulation

Based on the photino electronegativity $q_p < 0$ established in **Hypothesis I** and the electron-photino interaction mechanism established in **Hypothesis II**, the Coulomb repulsion between the electron and the photinos circulating around it provides the necessary centripetal force to maintain the circulation. The dynamical equilibrium equation is:

$$\boldsymbol{\frac{k_e e|q_p|}{r^2} = \frac{m_p v_p^2}{r}} \qquad \textbf{(2.4)}$$

Here, the circulation radius r is constrained by the characteristic scale of the electron itself. This radius must be consistent with the electron characteristic scale $r_e (r_e \leq 10^{-22} m)$ deduced from hydrogen atomic spectra in Hypothesis II.

Physical Meaning: This equation establishes the dynamical condition for the stable existence of microscopic photino circulation, unifying the origin of electromagnetic interaction with the kinematics of the medium, providing a theoretical foundation for constructing a self-consistent

parameter system.

Unified Construction of the Associated Parameter System

1. Photino Circulation Velocity

Based on the electron radius constraint from **Hypothesis I** and the photino field dynamics from **Hypothesis II**, the linear circulation velocity of photinos can be directly derived from the balance of Coulomb and centripetal forces:

$$\boldsymbol{v_p = \sqrt{\frac{k_e e Q_{\frac{p}{m}}}{r}}} \qquad \textbf{(2.5)}$$

Taking the critical value of the electron radius $r_e = 1.0 \times 10^{-22}\mathrm{m}$ and substituting the calibrated photino charge-to-mass ratio parameter $Q_{\frac{p}{m}} = 3.3 \times 10^{-3}\mathrm{C/kg}$ from **Hypothesis I**, the average circulation velocity of photinos near the "surface" of the electron spin axis can be calculated:

$$\boldsymbol{v_p \approx 2.18 \times 10^5 \mathrm{m/s}}$$

2. Photino Circulation Angular Velocity

From the relation between linear velocity and radius, the angular velocity corresponding to this circulation can be further calculated:

$$\boldsymbol{\omega_p = \frac{v_p}{r_e} \approx 2.18 \times 10^{27} \mathrm{rad/s}}$$

3. Dynamical Correlation between Electron Motion and Photino Circulation

Considering the characteristic motion velocity of electrons in atoms (e.g., the first Bohr orbital velocity):

$$\boldsymbol{v_e = \alpha c_0 \approx 2.18 \times 10^6 \mathrm{m/s}}$$

where α is the fine-structure constant and c_0 is the speed of light in vacuum. Thus, the ratio of photino circulation velocity to the characteristic electron motion velocity is:

$$\boldsymbol{\frac{v_p}{v_e} \approx 0.1}$$

Physical Meaning: This ratio (~0.1) intuitively reflects the **efficiency scale** of the conversion from electron translational momentum to photino circulation momentum. It demonstrates the energetic plausibility of the "electron motion dragging photinos" mechanism and confirms the principle that an isolated stationary electron cannot sustain directional circulation — the persistence of circulation requires continuous energy input from electron motion.

Deeper Implications:

- **Characterization of Spin****: Photino circulation is the **dynamical embodiment** of the electron's intrinsic spin angular momentum. Its circulation velocity and angular velocity concretely characterize the physical process of spin.

- **Correlation with the Magnetic Field**: This circulation velocity is directly related to the strength of the generated magnetic field, providing a crucial microscopic input parameter for the quantitative study of magnetic interactions.
- **Theoretical Self-Consistency**: The electron radius $r_e \approx 1 \times 10^{-22}\mathrm{m}$ used here is mutually consistent with the electron characteristic scale deduced independently from spectral analysis in **Hypothesis II**, forming cross-hypothesis parameter verification that enhances the overall self-consistency of the theory.

2. Microscopic Reconstruction and Unification of the Electron Magnetic Moment

Based on the photino circulation model established earlier, this section aims to reconstruct the fundamental physical quantity of the electron magnetic moment at the microscopic level. By establishing a direct connection between the intrinsic angular momentum of the electron and the photino circulation, we reduce the expression for the electron magnetic moment in quantum mechanics to a physical picture based on medium dynamics and achieve self-consistent verification of key parameters.

Angular Momentum Conservation and Coupled Photino Mass

According to the photino circulation motion described by Equation (2.3), the total spin angular momentum $\vec{S}$ of the electron is carried by the total orbital angular momentum of the n_p photinos coupled to it. This relationship can be expressed as the angular momentum conservation equation:

$$\vec{\boldsymbol{S}} = \sum_{i=1}^{n_p} \vec{\boldsymbol{L}}_{\boldsymbol{p}}^{(i)} = \boldsymbol{n_p m_p v_p r_e \hat{S}} = \boldsymbol{n_p m_p \omega_p r_e^2 \hat{S}}$$

Substituting the quantization condition from Equation (2.1), $S = \frac{\sqrt{3}\hbar}{2}$, yields the expression for the total mass of photinos coupled to a single electron:

$$\boldsymbol{n_p m_p = \frac{\sqrt{3}\hbar}{2\omega_p r_e^2}} \qquad \textbf{(2.6)}$$

Substituting $\omega_p \approx 2.18 \times 10^{27}\mathrm{rad/s}$ and $r_e = 1.0 \times 10^{-22}\mathrm{m}$ for calculation:

$$\boldsymbol{n_p m_p \approx 4.19 \times 10^{-18}\mathrm{kg}} \qquad \textbf{(2.7)}$$

Photino Equivalent Charge and Efficiency Coefficient

Based on the photino charge-to-mass ratio relation $q_p = Q_{\frac{p}{m}} m_p$ established in **Hypothesis I**, the total equivalent charge of the coupled photinos can be further obtained:

$$\boldsymbol{n_p q_p = Q_{\frac{p}{m}} \cdot (n_p m_p) \approx 1.38 \times 10^{-20}\mathrm{C}} \qquad \textbf{(2.8)}$$

Physical Meaning: $n_p q_p \approx 1.38 \times 10^{-20}\mathrm{C} < e$ (electron charge). This result demonstrates the plausibility of the model from the perspective of charge quantity. It indicates that the equivalent photino charge required to drive the circulation motion is less than one electron charge. Most of the Coulomb potential energy of the electron charge is used to maintain the electron's own field structure, rather than driving the medium motion.

Defining the efficiency coefficient η as the ratio of the equivalent photino charge driving the circulation $n_p q_p$ to the electron charge e:

$$\boldsymbol{n_p q_p = \eta e}$$

Combining Equation (2.6) with the charge-to-mass ratio relation yields the theoretical expression for η:

$$\boldsymbol{\eta = \frac{\sqrt{3}\hbar \frac{Q_p}{m}}{2e\omega_p r_e^2}} \qquad \textbf{(2.8)}$$

Substituting numerical values for calculation:

$$\boldsymbol{\eta \approx 0.086}$$

Physical Meaning: The efficiency coefficient $\eta \approx 8.6\%$ carries profound physical significance. It quantitatively reveals the energy distribution ratio in the electron-photino coupling process: only about 8.6% of the electron charge's "effective component" is used to drive photinos to form directional circulation. The remaining approximately 91.4% i**s primarily consumed in overcoming the vacuum centripetal pressure of the background medium under the atomic gravitational field** to maintain a stable medium background distribution. This mechanism is consistent in physical essence with the vacuum centripetal pressure mechanism related to strong interactions discussed in the **Photino Hypothesis** series.

This ratio is highly consistent in order of magnitude with the velocity ratio $v_p/v_e \approx 0.1$ derived earlier. Together, they constitute dual evidence for the efficiency of energy transfer from electron motion to medium circulation kinetic energy. This self-consistency among parameters not only validates the plausibility of the coupling mechanism but also forms a deep-level theoretical connection with the Coulomb force balance mechanism in **Hypothesis I** and the energy quantization principle in **Hypothesis II**.

Microscopic Expression for the Electron Spin Magnetic Moment

In quantum mechanics, the electron's spin magnetic moment is expressed as:

$$\boldsymbol{\vec{\mu}_s = -\, g_s \frac{e}{2m_e}\vec{S}}$$

where $g_s \approx 2.00232$ is the Landé g-factor for the electron, reflecting relativistic quantum effects

[10]. Substituting the expression for the electron spin angular momentum $\vec{S}$ in terms of the photino circulation angular momentum, $\vec{S} = n_p m_p \omega_p r_e^2 \hat{S}$, we obtain the **microscopic medium expression** for the electron spin magnetic moment:

$$\vec{\boldsymbol{\mu}}_{\boldsymbol{s}} = -\, \boldsymbol{g}_{\boldsymbol{s}} \frac{\boldsymbol{e}}{\boldsymbol{2m_e}} \left(\boldsymbol{n_p m_p \omega_p r_e^2}\right) \hat{\boldsymbol{S}} \qquad \textbf{(2.9)}$$

Physical Meaning: Equation (2.9) accomplishes a transition from abstract operators to a concrete dynamical picture.

- **Origin of the Magnetic Moment:** It clearly indicates that the essence of the electron spin magnetic moment originates from the **collective circulation angular momentum** formed by the electron and its coupled photinos. The source of the magnetic field is not a point-like "magnetic charge" but rather this microscopic medium vortex motion.
- **Analogy with the Electric Field**: This expression establishes a perfect analogy with the origin of the electric field: just as charge is the source of the electric field （$\nabla \cdot \vec{E} = \rho/\varepsilon_0$）, **microscopic medium circulation angular momentum (equivalent to magnetic moment) is the source of the magnetic field** $\left(\nabla \times \vec{B} = \mu_0 \vec{J} + \ldots\right)$.
- **Theoretical Unification:** It unifies the phenomenological result of quantum mechanics (the electron magnetic moment) with the dynamical processes of the photino medium, providing a theory based on real medium interactions for understanding the microscopic physical origin of the spin magnetic moment.

3. The Unified Photino Association of Planck's Constant

The Planck constant h is the cornerstone of quantum mechanics, and its physical essence has always been a central issue in theoretical physics exploration. Within the framework of this theory, the Planck constant is endowed with a clear microscopic medium dynamical significance, establishing a direct connection between fundamental quantization conditions and the motion of the photino medium.

Microscopic Expression for Planck's Constant

Starting from the angular momentum conservation equation $n_p m_p v_p r_e = \frac{\sqrt{3}\hbar}{2}$ and $v_p = \omega_p r_e$, the microscopic expression for Planck's constant can be obtained:

$$\boldsymbol{h} = \frac{\boldsymbol{4\pi r_e^2 n_p m_p \omega_p}}{\sqrt{\boldsymbol{3}}} = \frac{\boldsymbol{4\pi r_e^2 n_p \omega_p Q_{\frac{p}{m}}}}{\sqrt{\boldsymbol{3}} \boldsymbol{q_p}} \qquad \textbf{(2.10)}$$

Consequently, the reduced Planck constant is:

$$\hbar = \frac{2r_e^2 n_p \omega_p Q_{\frac{p}{m}}}{\sqrt{3} q_p} \qquad (2.11)$$

In-Depth Analysis of Physical Significance

This expression reveals the deeper physical connotation of Planck's constant:

- Electron Geometric Characteristic: The term $4\pi r_e^2$ represents the **characteristic area** of the electron spin circulation, associated with the electron characteristic scale D_e established in **Hypothesis II**.
- **Quantization of Coupling Strength**: The parameter n_p indicates the **quantum coupling strength** between a single electron and photinos, i.e., the number of photinos participating in the circulation.
- **Intrinsic Medium Property**: m_p is the photino mass, and its corresponding charge $q_p = Q_{\frac{p}{m}} m_p$ remains constant, reflecting the fundamental attributes of photinos.
- **Dynamical State:** ω_p is the angular velocity of the photino circulation, determined by the intrinsic spin properties of the electron, directly embodying the dynamics of the circulation.

Numerical Verification

Substituting the known parameters into Equation (2.10) for numerical calculation:

$$\boldsymbol{h = [4\pi \times (1.0 \times 10^{-22})^2 \times 4.19 \times 10^{-18} \times 2.18 \times 10^{27}] \div \sqrt{3}}$$

$$\boldsymbol{\approx 6.627 \times 10^{-34} kg \cdot m^2 \cdot s^{-1} (\text{or } J \cdot s)}$$

The calculated result is highly consistent with the experimental value, numerically verifying the correctness of this theory.

Unification with the Quantization Mechanism of Hypothesis II

This expression, together with the photon energy formula $E_\gamma = h\nu = m_\gamma c_0^2$ from Hypothesis II, constitutes a complete chain of quantization:

- **Quantization of Electron Spin Angular Momentum** → Microscopic expression of Planck's constant (Equation 2.10)
- **Quantization of Photon Energy** → Macroscopic manifestation of Planck's constant

This correspondence achieves a deep-level unification between microscopic quantization mechanisms and macroscopic quantum phenomena within the photino theoretical framework.

Microscopic Interpretation of the Biot-Savart Law and the Mechanism of Magnetic Field Action

1. Microscopic Expression of the Biot-Savart Law

The Biot-Savart law in classical electromagnetism describes the law of magnetic field generation by a current:

$$\vec{\boldsymbol{B}}_{\boldsymbol{macro}} = \frac{\boldsymbol{\mu_0}}{\boldsymbol{4\pi}} \boldsymbol{I} \int \frac{\boldsymbol{d\vec{l}} \times \hat{\boldsymbol{r}}}{\boldsymbol{r^2}}$$

The microscopic essence of a macroscopic current is the directional motion of a large number of electrons, defined as:

$$\boldsymbol{I} = \iint_{\boldsymbol{S}} \vec{\boldsymbol{J}} \cdot \boldsymbol{d\vec{S}} = \boldsymbol{n_e e S v_e}$$

where $\vec{J} = n_e e \vec{v}_e$ is the current density vector (n_e is the electron number density, v_e is the electron drift velocity).

Combining this with the electron magnetic moment equivalent charge equation $e = \frac{n_p q_p}{\eta}$, and linking the three expressions yields the microscopic expression of the Biot-Savart law:

$$\vec{\boldsymbol{B}}_{\boldsymbol{macro}} = \frac{\boldsymbol{\mu_0}}{\boldsymbol{4\pi}} \frac{\boldsymbol{n_p q_p}}{\boldsymbol{\eta}} \boldsymbol{n_e S v_e} \int \frac{\boldsymbol{d\vec{l} \times \hat{r}}}{\boldsymbol{r^2}} \qquad \textbf{(2.12)}$$

Physical Meaning: This law describes the collective magnetic field effect of the photino helical circulation excited by a large number of moving electrons. Within the photino theory framework, the magnetic effect of a macroscopic current receives a microscopic explanation: a macroscopic magnetic field is essentially the vector superposition of the photino circulation magnetic fields excited by N_e electrons:

$$\vec{\boldsymbol{B}}_{\boldsymbol{macro}} = \sum_{\boldsymbol{i=1}}^{\boldsymbol{N_e}} \vec{\boldsymbol{B}}_{\mathbf{mag}}^{(\boldsymbol{i})} = \frac{\boldsymbol{\mu_0}}{\boldsymbol{4\pi}} \int \frac{\vec{\boldsymbol{J}}_{\boldsymbol{macro}} \times \hat{\boldsymbol{r}}}{\boldsymbol{r^2}} \boldsymbol{dV}$$

2. The Essence of the Torque Exerted by a Magnetic Field on a Magnetic Moment

The expression for the torque exerted by a magnetic field on a magnetic moment is:

$$\vec{\boldsymbol{M}} = \vec{\boldsymbol{\mu}} \times \vec{\boldsymbol{B}}, \boldsymbol{M} = \boldsymbol{\mu B} \mathbf{sin} \boldsymbol{\theta}$$

where θ is the angle between $\vec{\mu}$ and $\vec{B}$.

Physical Meaning: In photino theory, the essence of the magnetic torque is the angular momentum exchange resulting from the Coulomb force interaction between the photino circulations corresponding to the external magnetic field $\vec{B}$ and the magnetic moment $\vec{\mu}$. This exchange produces a net torque, causing the magnetic moment to align with the lower energy state along the direction of the external field. This microscopic angular momentum transfer process obeys angular momentum conservation. Its macroscopic manifestation is equivalent to the

classical magnetic torque formula, achieving a unified description of medium dynamics and macroscopic magnetic phenomena.

Summary

This section, based on the unified photino field theory framework, establishes a microscopic circulation model for the sourceless magnetic field. The theory indicates that the essence of the magnetic field is the helical circulation effect formed by moving electrons driving photinos through coordinated spin-velocity action. Through rigorous mathematical derivation, a self-consistent parameter system centered on the angular velocity $\omega_p \approx 2.18 \times 10^{27}\mathrm{rad/s}$ and the efficiency coefficient $\eta \approx 0.086$ has been established. Key parameters such as the photino equivalent charge $n_p q_p \approx 1.38 \times 10^{-20}\mathrm{C}$ have been successfully derived.

Theoretical verification shows that the microscopic expression for Planck's constant, $h = 4\pi r_e^2 n_p m_p \omega_p/\sqrt{3}$, is in high agreement with the experimental value, achieving a deep unification of **Hypothesis I**, **II**, in terms of both parameter system and physical mechanism. Simultaneously, classical electromagnetic laws (such as the Biot-Savart law and the magnetic torque formula) have obtained microscopic explanations based on medium dynamics within this framework, laying a solid theoretical foundation for the complete description from microscopic particle interactions to macroscopic magnetic phenomena.

2.1.3 Source Magnetic Field: Dynamic Equilibrium of the Transient Photino Flow Field

The source magnetic field, i.e., the magnetic field component satisfying $\nabla \times \vec{B} = \mu_0 \vec{J} + \mu_0 \varepsilon_0 \frac{\partial \vec{E}}{\partial t}$, is interpreted at the microscopic level as **a transient flow field formed by the directional acceleration of photinos driven by a time-varying electric field via the Coulomb force**. This mechanism shares the same physical foundation as the vertical plate experiment established in **Photino Hypothesis I** to explain the gravitational field [1], namely, the collective dynamical response of photino electronegativity under a non-static electric field.

Physical Model and Dynamical Equations

1. **Parallel Plate System Configuration:**

- Consider a parallel-plate capacitor with a plate separation d, to which a time-varying voltage $U(t)$ is applied.
- The resulting time-varying electric field strength between the plates is $E(t) = U(t)/d$, directed from the positive to the negative plate.
- Photinos carry a negative charge $q_p < 0$, possess mass m_p, and their initial number density

distribution $n_{p0}(\vec{r})$ follows the law established in **Hypothesis I**.

2. Force Analysis and Dynamical Equation:

The photinos between the plates experience a driving force from the time-varying electric field and a damping force arising from their motion through the medium. Their equation of motion can be written as:

$$\boldsymbol{m_p \frac{dv_p}{dt} = q_p E(t) - \eta v_p} \qquad \textbf{(2.13)}$$

Here, $\eta$is the damping coefficient, which is related to the characteristic time constant $\tau_2 = a^2/D_p$ describing photino diffusion behavior in **Hypothesis I.**

Transient Process Analysis and Experimental Verification

1. Phased Dynamical Behavior:

- **Transient Acceleration Phase** $(t \approx 0)$: The electric force $q_p E(t)$ dominates, and the photino velocity v_p increases approximately linearly.
- **Dynamic Equilibrium Phase** $(0<t<\tau)$: As velocity increases, the damping force ηv_p strengthens, the photino acceleration decreases, and the velocity approaches its peak value.
- **Steady-State Phase** $(t \to \infty)$: For a constant electric field, the electric and damping forces eventually balance, resulting in zero net acceleration and cessation of directional photino flow.

2. Microscopic Interpretation of Displacement Current:

The Maxwell displacement current density $J_d = \varepsilon_0 \frac{\partial E}{\partial t}$ acquires a clear physical entity in this model. It is essentially the equivalent current of the photino flow driven by the time-varying electric field:

$$\boldsymbol{J_d = \varepsilon_0 \frac{\partial E}{\partial t} = n_{p0} q_p v_p = n_{p0} q_p \int_0^t \frac{F_{\text{net}}(t')}{m_p} dt'} \qquad \textbf{(2.14)}$$

where $F_{\text{net}}(t') = q_p E(t') - \eta v_p(t')$. Combining this with the relationship between the speed of light and vacuum electromagnetic constants established in **Hypothesis II**, $c_0 = 1/\sqrt{\varepsilon_0 \mu_0} = \sqrt{aS/2}$, yields:

$$\boldsymbol{\varepsilon_0 = \frac{2}{aS\mu_0}}$$

This indicates that the vacuum permittivity ε_0 fundamentally reflects the intrinsic dynamical properties of the spacetime photino field.

3. **Experimental Correlation and Verification Scheme** (as shown in Figure 2.2):

- An apparatus similar to the vertical plate experiment in **Hypothesis I** can be used, replacing the test sphere with a high-sensitivity magnetometer (e.g., a SQUID).
- Observe the build-up and decay process of the magnetic field in the gap between the plates after applying a transient voltage pulse, verifying the theoretically predicted temporal evolution $B(t) \propto J_d(t) \propto v_p(t)$.
- **Direction Specificity Verification**: This theory provides a crucial, testable prediction—the observed magnetic field direction is directly determined by the photino flow direction. Specifically, reversing the electrode polarity will reverse the photino flow direction, consequently causing a synchronous reversal of the observed magnetic field direction. This unique causal relationship serves as an important criterion distinguishing it from other potential mechanisms.

Theoretical Unity and Parameter Self-Consistency

1. **Parameter Prediction and Experimental Constraint:**

Based on the model, the temporal characteristics of the magnetic field decay (or build-up) process can provide experimental constraints on photino parameters. From the dynamical equation, it can be deduced that the magnetic field decay time constant τ_2 has a quantitative relationship with the photino charge-to-mass ratio and number density:

$$\boldsymbol{\frac{q_p}{m_p} = \frac{4\pi\varepsilon_0 B_{\max}}{n_{p0} E_0 \tau_2}}$$

Combining this with the charge-to-mass ratio relation $\frac{q_p}{m_p} = Q_{\frac{p}{m}}$ established in **Hypothesis I**, the model predicts a quantitative relationship between the magnetic relaxation time τ_2, the photino number density n_{p0}, and the maximum magnetic field strength B_{max}:

$$\boldsymbol{\tau_2 \approx \frac{4\pi\varepsilon_0 B_{\max}}{n_{p0} E_0 Q_{\frac{p}{m}}}}$$

This explicit theoretical prediction provides a clear experimental pathway for determining or constraining the intrinsic photino parameters (e.g., q_p, m_p, n_{p0}) through precise magnetic measurements in the future.

2. **Qualitative Self-Consistency with Hypothesis I:**

- The photino electronegativity $(q_p < 0)$ on which this model relies is consistent with the qualitative conclusions of the vertical plate experiment in **Hypothesis I**.
- The relaxation time scale（τ_2）in the model is consistent in order of magnitude with the

transient mechanical response time observed in **Hypothesis I**, indicating both originate from the dynamical properties of the same medium.

Conclusion

The essence of the source magnetic field is the transient flow field formed by photinos driven by a time-varying electric field. The discussion in this section achieves the following core advancements:

1. **Mechanistic Unity**: It reduces the "displacement current" term in Maxwell's equations to the dynamical process of photino flow, providing an intuitive microscopic physical picture for this key concept.
2. **Theoretical Self-Consistency:** The model is fully compatible with the spacetime medium framework and parameter system established in **Photino Hypotheses I and II**. Parameters such as $Q_{p/m}, \varepsilon_0$ achieve a cross-hypothesis unified interpretation.
3. **Technical Foresight:** The theory predicts that optimizing the electric field rate of change (e.g., using high-voltage fast-pulse power supplies) and the plate geometry (e.g., reducing spacing d, increasing area) can effectively enhance the transient photino flow intensity. This opens a new principle-based pathway for developing **novel pulsed high-magnetic-field technology** based on electric field excitation rather than large-current solenoids.
4. **Testability**: The theory provides explicit predictions testable through precise magnetic measurements (e.g., magnetic field direction reversal, quantitative relationship between relaxation time and field strength), pointing the way for subsequent quantitative experimental research.

This theoretical framework provides a new microscopic foundation for understanding the source magnetic field. Its correctness **awaits experimental verification** by future precise experiments focusing on the transient magnetic field process, while simultaneously laying a theoretical foundation for exploring entirely new schemes for generating strong magnetic fields."

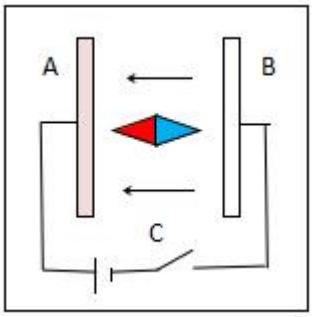

Fig.2.2

2.2 Microscopic Mechanism of Magnetic Forces

Building upon the interpretation of the magnetic field's essence as a photino flow field, this section aims to provide a microscopic explanation based on medium dynamics for the fundamental magnetic forces in classical electromagnetism—the **Lorentz force** and the **Ampere force**—as well as the interaction forces between magnetic poles. This theory groundbreakingly

reduces magnetic forces to the effect of **Coulomb pressure difference** caused by photino density gradients, thereby achieving a unified understanding of macroscopic magnetic forces at the level of microscopic particle interactions.

2.2.1 Lorentz Force and Ampere Force

The Photino Pressure Difference Mechanism of the Lorentz Force

Physical Picture and Microscopic Mechanism: Consider the case where an electron moves with velocity $\vec{v}_e$ perpendicular to an external magnetic field $\vec{B}$ (as shown in Figure 2.3). According to the model in Section 2.1, the external magnetic field corresponds to a background photino flow in a specific direction. Due to the chiral (left-handed) spin characteristic of the electron, the microscopic photino circulation it excites interacts with the background flow, causing an asymmetry in the local photino distribution around the electron.

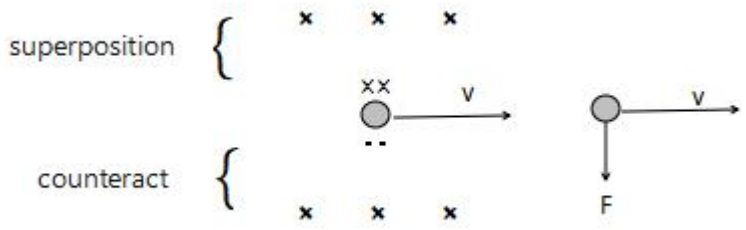

Fig. 2.3

1. **Region Above the Electron**: The microscopic magnetic field $\vec{B}$ generated by the electron's spin aligns with the direction of the external magnetic field $\vec{B}$, causing the photino flows in this region to cooperate with each other. This increases the number density $n_{p0}^{(\text{upper})}$ and decreases the average spacing r_{upper}. According to Coulomb's law, this forms a **high-pressure region**, and the Coulomb repulsive force F_{upper} on the electron from this direction is enhanced:

$$\boldsymbol{F_{\text{upper}} = \frac{k_e\left(Q_p^{(\text{upper})}\right)^2}{r_{\text{upper}}^2}}, \quad \text{where} \quad \boldsymbol{Q_p^{(\text{upper})} = V \cdot n_{p0}^{(\text{upper})} q_p}$$

2. **Region Below the Electron**: The electron's spin magnetic field $\vec{B}_{\text{spin}}$ is opposite to the direction of the external magnetic field $\vec{B}$. The two photino flows collide head-on, producing a repulsive expulsion effect. This decreases the photino number density $n_{p0}^{(\text{lower})}$ in this region and increases the average spacing r_{lower}. This forms a **low-pressure region**, and the Coulomb repulsive force F_{lower} on the electron from this direction is weakened:

$$F_{\text{lower}} = \frac{k_e\left(Q_p^{(\text{lower})}\right)^2}{r_{\text{lower}}^2}$$

3. **Net Pressure and Lorentz Force:** The pressure difference in Coulomb repulsion from the upper and lower regions causes the electron to be deflected to one side. Macroscopically, this manifests as the Lorentz force:

$$\vec{F}_{\text{Lorentz}} = \vec{F}_{\text{upper}} - \vec{F}_{\text{lower}} = q_e\vec{v}_e \times \vec{B} \qquad (2.17)$$

Its direction is determined by the classical left-hand rule.

4. **Correlation with Experiment:** This model naturally explains the linear dependence of the Lorentz force on electron velocity. An increase in electron velocity v_e → enhances its spin magnetic moment → increases the resulting photino density gradient $\Delta n_{p0} \propto v_e$ → ultimately manifests as a linear enhancement of the Lorentz force $F \propto v_e$.

Ampere Force: The Statistical Manifestation from Microscopic Lorentz Force to Macroscopic Force

The Ampere force is essentially the collective effect of the Lorentz forces experienced by a large number of free electrons in a conductor, with momentum transfer occurring through electron-lattice collisions.

1. **Collective Lateral Deflection of Free Electrons**: Each free electron in the conductor acquires a lateral acceleration $a_\perp = F_{\text{Lorentz}}/m_e = q_e v_0 B/m_e$ under the Lorentz force. Over a characteristic length L along the conductor, its accumulated lateral velocity is:

$$v_\perp = a \cdot t = \frac{q_e v_0 B}{m_e} \cdot \frac{L}{v_0} = \frac{q_e B L}{m_e}$$

2. **Accumulation of Lateral Momentum:** Let the total number of free electrons participating in conduction in the conductor be N_e. The total lateral momentum generated is:

$$\Delta p = N_e m_e v_\perp = N_e q_e B L$$

3. **Lattice Collisions and Macroscopic Force Manifestation**: Electrons collide with lattice atoms, transferring lateral momentum to the lattice. Let the average collision time interval be τ. The rate of momentum transfer, i.e., the Ampere force manifested macroscopically, is:

$$F_{\text{Ampere}} = \frac{\Delta p}{\tau} = \frac{N_e q_e B L}{\tau} = IBL\left(\text{where } I = \frac{N_e q_e}{\tau}\right) \qquad (2.18)$$

Physical Meaning: Equation (2.18) clearly indicates that **the Ampere force is the statistical average effect manifested after the microscopic Lorentz forces on a large number of electrons transfer momentum through lattice collisions**. The greater the current I or the stronger the external magnetic field B, the greater the collective lateral momentum transferred by electrons per unit

time, and the more significant the macroscopic Ampere force.

2.2.2 Interaction Forces Between Magnetic Poles

Within the framework of photino theory, the attractive and repulsive forces between magnetic poles stem from the interactions between photino flows excited by poles of different orientations. These interactions can be microscopically described through the **Coulomb pressure difference** mechanism, thereby providing a unified picture of magnetic pole interactions based on medium dynamics.

Repulsive Force Between N-Poles

When the N-poles of two magnets approach each other (as shown in Figure 2.4), the microscopic process is as follows:

1. **Head-on Collision of Photino Flows**: Each N-pole radiates a helical photino flow in a specific direction. When two N-poles approach, their emitted flows collide head-on.
2. **Density Surge and Pressure Increase in the Collision Zone**: The collision causes photinos to accumulate in the local region, sharply increasing the number density $n_p^{(\text{collision})}$ and significantly decreasing the average spacing $r_{\text{collision}}$. According to Coulomb's law $F \propto 1/r^2$, a decrease in spacing leads to a sharp increase in repulsive force.
3. **Inverse-Square Law Manifestation of Repulsion:** The repulsive force originates from the difference between the additional Coulomb pressure generated by the high-density photinos in the collision zone and the background pressure:

$$\boldsymbol{F_{\text{rep}} = F_{\text{collision}} - F_{\text{background}} = \frac{k_e Q_{\text{collision}}^2}{r_{\text{collision}}^2} - \frac{k_e Q_{\text{background}}^2}{r_{\text{background}}^2} \left(r_{\text{collision}} \ll r_{\text{background}}\right)} \quad \textbf{(2.19)}$$

This constitutes the microscopic mechanism behind the inverse-square law obeyed by magnetic pole repulsion.

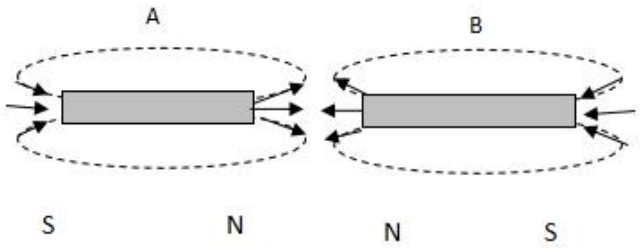

Fig.2.4

Repulsive Force Between S-Poles

Physically, an S-pole corresponds to the direction of photino flow reflux (as shown in Figure 2.5). When two S-poles approach:

- **Mechanism**: Two oppositely directed reflux photino flows also form a collision scenario. The

microscopic mechanisms of collision, accumulation, and repulsion generation are identical to the N-N pole case.

- **Formula:** The expression for the repulsive force is formally identical to Equation (2.19).

  Therefore, the repulsion between S-S poles and N-N poles **stem from the same microscopic mechanism** in photino theory.

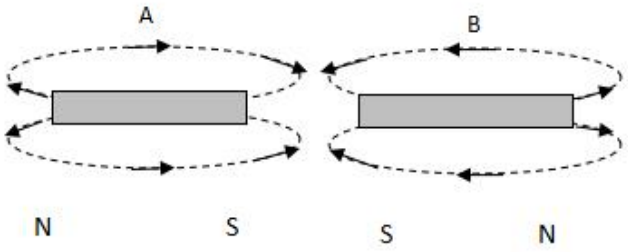

Fig.2.5

Attractive Force Between N and S Poles

When the N-pole of one magnet approaches the S-pole of another (as shown in Figure 2.6), **the dynamical process differs from the repulsive case**:

1. **Formation of Coordinated Photino Flow**: When the emitted photino flow from the N-pole of magnet A meets the reflux from the S-pole of magnet B in space, they tend to form a **coordinated flow in the same direction**, constituting a circulatory path.
2. **Velocity Increase and Spacing Increase:** Coordinated flow reduces resistance, leading to an increase in the overall photino flow velocity v_p in this region. The velocity increase is accompanied by an increase in the average particle spacing $r_{\text{coord}}(r_{\text{coord}} \propto v_p)$.
3. **Coulomb Pressure Difference Generating Attraction:** The increased spacing in the coordinated flow region results in a lower Coulomb repulsive force F_{coord} compared to that in the background region $F_{\text{background}}$. This pressure difference manifests as a net attractive force:

$$\boldsymbol{F_{\text{attr}} = \frac{k_e q_p^2}{r_{\text{background}}^2} - \frac{k_e q_p^2}{r_{\text{coord}}^2} \left(r_{\text{coord}} > r_{\text{background}}\right)} \qquad \textbf{(2.20)}$$

4. **Establishment of a Stable Circulation**: Ultimately, photinos can establish a stable macroscopic circulation along the path N-pole → S-pole → N-pole, corresponding to the combined magnetic field distribution of the two magnets in equilibrium.

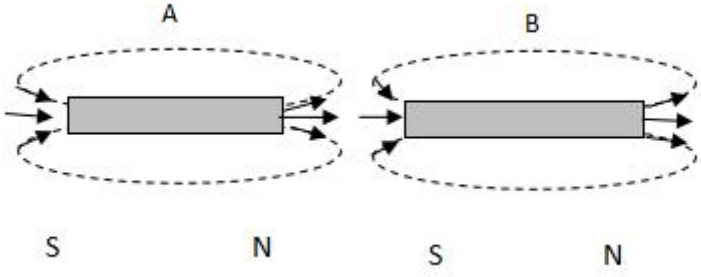

Fig.2.6

Mechanism for Repulsion Being Greater Than Attraction

Experiments show that the repulsive force between identical magnets is typically slightly greater than the attractive force. This can be explained within the photino pressure difference model:

- For **repulsion** (N-N or S-S), it stems from **head-on collision and accumulation** of photinos, causing a sharp decrease in spacing r ($\Delta r_{\text{rep}} < 0$). Due to $F \propto 1/r^2$, the decrease in spacing has a significant impact on the force magnitude.
- For **attraction** (N-S), it stems from **coordinated flow and rarefaction** of photinos, causing an increase in spacing r ($\Delta r_{\text{attr}} > 0$).
- Under identical conditions, the magnitude of spacing decrease caused by collision $|\Delta F_{\text{rep}}|$ is typically greater than the magnitude of spacing increase caused by coordinated flow $|\Delta F_{\text{tattr}}|$. Therefore, the rate of force change determined by Equations (2.19) and (2.20) satisfies:

$$\left|\frac{\boldsymbol{\Delta F_{\text{rep}}}}{\boldsymbol{\Delta r}}\right| > \left|\frac{\boldsymbol{\Delta F_{\text{attr}}}}{\boldsymbol{\Delta r}}\right|$$

This explains, at the mechanistic level, why repulsion is generally more pronounced.

Experimental Verifiability

The microscopic mechanisms of magnetic forces elaborated in this chapter can all be validated through experiments:

- **Lorentz Force Verification:** Verify the relationship $F \propto v$ by measuring the deflection of electrons with different velocities in a uniform magnetic field.
- **Magnetic Pole Interaction Force Verification**: Precisely measure the variation of the interaction force between magnets with distance, verify the inverse-square law $F \propto 1/r^2$, and compare the magnitudes of repulsive and attractive forces at the same distance.

Summary

Through the photino density gradient and Coulomb pressure difference mechanism, this section constructs a self-consistent theoretical framework connecting microscopic dynamics to macroscopic magnetic forces:

1. **Unified Mechanism**: The Lorentz force on moving charges, the Ampere force on current-carrying conductors, and the attractive/repulsive forces between magnetic poles are all unified under the core physical picture of **Coulomb pressure imbalance caused by uneven photino density distribution**.
2. **Predictive and Explanatory Power:** The theory, based on photino parameters, can explain the directional dependence, magnitude dependencies (e.g., on velocity and distance), and phenomena like repulsion being greater than attraction.
3. **Consistency of the Parameter System**: All derivations are closely tied to the parameter system (e.g., $q_p, Q_{\text{q/m}}, n_{p0}$) established in **Photino Hypotheses I and II**, ensuring the internal unity

and logical coherence of the entire theoretical framework. This provides a new fundamental physical perspective for the analysis and design of electromagnetic devices (e.g., motors, maglev systems).

2.3 Microscopic Mechanism of Magnetic Induction

Based on the established nature of the magnetic field as a photino flow field within the photino hypothesis, this section systematically elaborates the microscopic physical mechanism of electromagnetic induction phenomena. Unlike classical electromagnetic theory, which treats magnetic induction as a mathematical description based on field lines, this theory reduces Faraday's law of electromagnetic induction to the effect of a **Coulomb pressure difference caused by photino density gradients**, achieving a theoretical leap from macroscopic phenomenological description to microscopic physical mechanism.

2.3.1 Fundamental Principles

The physical essence of electromagnetic induction is uniformly explained in this theory as a **dynamic process where changes in photino density gradients, induced by an external magnetic field or conductor motion, lead to an imbalance of forces on electrons**. This pressure difference mechanism provides a unified microscopic foundation for understanding the complete spectrum of phenomena from motional electromotive force (EMF) to induced EMF.

Physical Picture and Shift in Microscopic Mechanism

- **Electron Motion Without an External Magnetic Field**: When free electrons move within a conductor, the surrounding photino background is uniformly distributed. Collisions between electrons and photinos do not produce a sustained net pressure difference, and thus no induced current manifests macroscopically.
- **Shift in Mechanism Upon Applying an External Field or Conductor Motion:**

1. **External Magnetic Field Establishes Directional Circulation**: An external magnetic field $\vec{B}$ corresponds to a background photino directional circulation with specific momentum.
2. **Change in Electron-Photino Collision Dynamics**: When electrons move within the conductor, they collide with these directionally moving photinos. Directionally flowing photinos are less easily pushed aside by electrons compared to a disordered background, altering the momentum exchange characteristics of the collisions.
3. **Formation of Asymmetric Density Gradient:** The electrons "compress" photinos ahead of their motion, leading to an increase in the local photino number density and a decrease in spacing r_{front}. Behind their motion, they "stretch" the photino distribution, causing a decrease in number density and an increase in spacing r_{back} (as shown in Figure 2.7).
4. **Generation of Coulomb Pressure Difference:** The difference in photino density ahead and behind the electron creates an imbalance in the Coulomb repulsive force experienced by the electron, with greater pressure from the front than from the back.
5. **Collective Electron Deflection and Induced Current**: This net pressure drives the free

electrons in the conductor to undergo collective directional deflection, leading to charge accumulation at the conductor ends and the generation of an induced electromotive force.

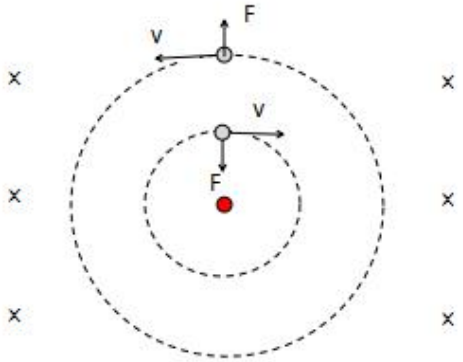

Fig.2.7

Mathematical Formulation

The net Coulomb pressure acting on a single electron originates from the difference in photino spacing ahead and behind it. Let the average background spacing be r_0, and the change in spacing induced by the external magnetic field or relative motion be Δr, so that $r_{\text{front}} = r_0 - \Delta r$ and $r_{\text{back}} = r_0 + \Delta r$. According to Coulomb's law, the net pressure F_{net} can be expressed as:

$$\boldsymbol{F_{\text{net}}} = \left|\frac{\boldsymbol{k_e q_p^2}}{\boldsymbol{r_{\text{front}}^2}} - \frac{\boldsymbol{k_e q_p^2}}{\boldsymbol{r_{\text{back}}^2}}\right| \approx \frac{\boldsymbol{4k_e q_p^2 \Delta r}}{\boldsymbol{r_0^3}} \qquad (2.21)$$

Here, the spacing change Δr is proportional to the electron's velocity relative to the magnetic field v_e and the magnetic field strength B (which is proportional to the background photino flow density), i.e., $\Delta r \propto v_e B$. Therefore, the net pressure satisfies $F_{\text{net}} \propto v_e B$, which is consistent in its physical dependencies with the macroscopic form of the Lorentz force $F = q_e v_e B$.

This pressure difference model explicitly correlates the abstract mathematical concept of "change in magnetic flux" with **spatial gradient changes in photino momentum flux**, providing a realistic interpretation of the law of electromagnetic induction based on medium interactions.

2.3.2 Microscopic Process of a Conductor Cutting a Magnetic Field

This section, based on the photino density gradient pressure difference model, provides a detailed analysis of the dynamical process through which an electromotive force (EMF) is generated when a conductor moves within a magnetic field. The entire process can be divided into three stages: orbital energy level separation (Zeeman effect), photino flow-electron collision dynamics, and the final pressure difference formation and electron deflection.

Definition of the Three-Dimensional Coordinate System and Physical Setup

To clearly describe this process, a three-dimensional coordinate system is established as shown in Figure 2.8:

- **Magnetic Field Direction**: Corresponds to the background photino flow direction, defined as perpendicularly into the page ($-z$ axis).
- **Conductor Motion Direction**: The conductor moves with velocity v along the $+y$ axis.
- **Electron Force Analysis**: Focuses on the behavioral changes of bound electrons within atoms in the conductor. Their eventual escape direction is along the $+x$ axis.

Stage One: Orbital Energy Level Separation (Zeeman Effect)

Under the influence of the external magnetic field, the orbital motion of electrons within atoms is first affected, leading to energy level splitting—the microscopic origin of the Zeeman effect.

- **Observation along the magnetic field direction ($-z$ axis)**: The circular motion of electrons around the atomic nucleus can be divided into clockwise (CW) and counterclockwise (CCW) directions.
- **Action of the Lorentz force**: According to Equation (2.17), a moving electron experiences a Lorentz force $F_L = q_e v_e \times B$. The direction of this force depends on the electron's velocity direction.
  - **Counterclockwise (CCW) moving electrons**: The Lorentz force points away from the nucleus, tending to increase the orbital radius（$r\uparrow$), lower the binding energy（$\Delta E > 0$), and make the electron more likely to become free.
  - **Clockwise (CW) moving electrons:** The Lorentz force points towards the nucleus, tending to decrease the orbital radius（$r\downarrow$）, increase the binding energy （$\Delta E < 0$）, and make the electron more bound.
- **Continuous chain of electron state transition**: This energy level splitting is the **prerequisite** for the transition of electrons from a bound state to a conduction state. The complete chain is: bound-state electron → Zeeman energy level splitting → change in orbital radius and binding energy → provides the dynamical basis for subsequent photino flow collisions leading to escape.

Stage Two: Photino Flow-Electron Collision Dynamics

When the conductor moves within the magnetic field, the electrons inside the conductor experience relative motion with respect to the background photino flow corresponding to the external magnetic field, resulting in collision interactions. As shown in Figure 2.8, the forces on electrons are considered within the four quadrants (A→B→C→D) defined relative to the atomic nucleus along the photino flow direction.

The equation for the electron's circular motion within the atom is:

$$\frac{Ze^2}{4\pi\varepsilon_0 r^2} = \frac{m_e v_e^2}{r} \pm f_p \qquad (2.22)$$

where:

- $\frac{Ze^2}{4\pi\varepsilon_0 r^2}$ is the Coulomb attractive force F_{attr} between the nucleus and the electron.
- $\frac{m_e v_e^2}{r}$ is the centrifugal force F_{cent} required for the electron's circular motion.
- f_p is the **reaction force** arising from collisions between the photino flow and the electron. Its direction depends on the specific position of the electron in its orbit (as illustrated), and its magnitude is related to the kinetic energy density of the photino flow, $f_p \propto n_p q_p E_p$.

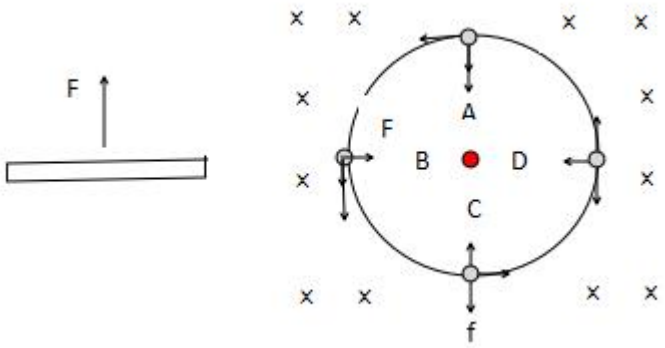

Fig.2.8

The analysis of force and orbital evolution for electrons in different quadrants is summarized in the table below:

Table 2.1: Analysis of Forces and Orbital Evolution for Electrons in the Four Quadrants

Orbital Region	Force Analysis	Net Force Direction	Orbital Evolution and Result
D→A	$F_{\text{attr}} > F_{\text{cent}} - f_p$	Towards the nucleus	Orbital contraction（r↓） tighter bound state
A→B	$F_{\text{attr}} > F_{\text{cent}} - f_p$	Towards the nucleus	Orbital contraction（r↓） tighter bound state
B→C	$F_{\text{attr}} < F_{\text{cent}} + f_p$	Away from the nucleus	Orbital expansion（r↑） possible escape
C→D	$F_{\text{attr}} < F_{\text{cent}} + f_p$	Away from the nucleus	Orbital expansion（r↑） possible escape

Critical Condition for Escape: For electrons in regions B→C and C→D, particularly the counterclockwise (CCW) electrons whose orbital radius has already increased due to the Zeeman effect, they will break free from atomic binding and become conduction electrons when the following condition is met:

$$\frac{Ze^2}{4\pi\varepsilon_0 r^2} < \frac{m_e v_e^2}{r} + f_p$$

The corresponding critical escape radius r_{crit} is:

$$r_{\text{crit}} = \frac{Ze^2}{4\pi\varepsilon_0\left(\frac{m_e v_e^2}{r} + f_p\right)} \qquad (2.23)$$

Stage Three: Pressure Difference Formation, Electron Deflection, and Induced EMF

The electrons that successfully escape or are affected subsequently move within the conductor and experience the net photino pressure described by Equation (2.21). For a conductor moving in the $+y$ direction, its internal electrons experience:

- **Ahead (+y direction)**: Photinos are "compressed," density increases（n_p ↑）, spacing r_{front} ↓, forming a high-pressure region.
- **Behind (-y direction)**: Photinos are "stretched," density decreases $(n_p \downarrow)$, spacing r_{back} ↑, forming a low-pressure region.

The resulting net pressure $F_{\text{net}} \propto v_e B$ drives electrons to deflect along the $+x$ direction, leading to charge accumulation at the conductor ends and the generation of a potential difference. For a conductor of length L, the induced electromotive force is:

$$\mathcal{E}_{\text{ind}} = \int_0^L \frac{F_{\text{net}}}{q_e} dy \propto v_e B L$$

This result is fully consistent with the motional EMF formula derived in classical electromagnetism from the Lorentz force $\vec{F} = q_e \vec{v}_e \times \vec{B}$.

Verification of the Right-Hand Rule: The process described above naturally yields the directional relationships of the right-hand rule:

1. **Magnetic Field Direction (palm):** $-z$ axis (photino flow direction).
2. **Conductor Motion Direction (thumb)**: +y axis.
3. **Induced Current Direction (fingers)**: -x axis (opposite to the electron flow direction +x). This is in complete agreement with the predictions of classical theory.

2.3.3 The Pressure Difference Model for the Three Key Factors of Magnetic Induction

Based on the aforementioned mechanism of photino density gradient and Coulomb pressure difference, the three decisive factors of magnetic induction (i.e., electromagnetic induction)—**cutting velocity v, magnetic field strength B, and conductor length L**—obtain a unified microscopic dynamical interpretation within this theoretical framework. This model directly links the macroscopic induced electromotive force \(\mathcal{E}\) to the microscopic change in

photino spacing Δr and the resulting net pressure F_{net}, thereby completing the theoretical construction from classical phenomenological description to a microscopic medium-based picture.

Microscopic Mechanism Correlation of the Three Factors

The table below systematically summarizes the physical roles and quantitative relationships of the three key factors in the photino pressure difference model:

Table 2.2: Interpretation of the Three Key Factors of Magnetic Induction via the Photino Pressure Difference Model

Factor	Photino Dynamical Mechanism	Mathematical Representation
Cutting Velocity v	The relative motion velocity v between the conductor and the magnetic field directly determines the degree to which electrons "compress" or "stretch" the photino medium, thereby linearly modulating the change in photino spacing: $\Delta r \propto v$	$\varepsilon \propto v$
Magnetic Field Strength B	The magnetic field strength B is proportional to the density and momentum of the background photino directional circulation. A larger B corresponds to a stronger background flow, leading to a stronger interaction with moving electrons, resulting in: $\Delta r \propto B$	$\varepsilon \propto B$
Conductor Length L	The conductor length L defines the path integral range over which the net pressure F_{net} does work on the electrons. Increasing the length extends the effective spatial scale for pressure difference accumulation.	$\varepsilon \propto L$

Integrating the above relationships, the induced electromotive force can be expressed as:

$$\boldsymbol{\varepsilon \propto vBL}$$

This expression is formally identical to the motional EMF formula in classical electromagnetism but is endowed with a clear connotation of microscopic medium interaction.

Pressure Difference Form of Faraday's Law of Electromagnetic Induction

For the more general case—where a time-varying magnetic field $\frac{\partial \vec{B}}{\partial t} \neq 0$ induces an EMF in a stationary loop—the photino pressure difference model also provides a natural explanation. In this case, the change in the magnetic field directly causes variations in the background photino flow density n_p and momentum $n_p q_p \vec{v}_p$ at points in space.

Following the physical concept of Equation (2.21), the induced EMF originates from the work done by the line integral of the net pressure field along the closed loop C. When the photino density gradient changes with time, the net pressure field $\frac{\vec{F}_{\text{net}}(\vec{r},t)}{q_e}$ becomes a time-dependent vector field. The induced EMF equals the line integral of this field along the loop:

$$\boldsymbol{\varepsilon(t) = \oint_C \frac{\overrightarrow{F_{\text{net}}(\vec{r},t)}}{q_e} \cdot d\vec{l}}$$

Since $\vec{F}_{\text{net}} \propto \nabla(n_p q_p \vec{v}_p)$ and the magnetic field $\vec{B} \propto n_p q_p \vec{v}_p$, applying Stokes' theorem from vector calculus transforms the above equation into a surface integral over the area S bounded by the loop:

$$\boldsymbol{\varepsilon(t) = -\frac{\partial}{\partial t}\iint_S (n_p q_p \vec{v}_p)\cdot d\vec{A} \propto -\frac{\partial}{\partial t}\iint_S \vec{B}\cdot d\vec{A}}$$

That is:

$$\boldsymbol{\mathcal{E} = -\frac{d\Phi_B}{dt}} \qquad \textbf{(2.24)}$$

where $\Phi_B = \iint_S \vec{B}\cdot d\vec{A}$ is the magnetic flux through the area bounded by the loop.

Physical Meaning: The derivation of Equation (2.24) reveals that the microscopic essence of the "rate of change of magnetic flux" in Faraday's law is **the time rate of change of the net photino momentum flux within the region enclosed by the loop**. This interpretation reduces the abstract concept of "magnetic flux" to a process of momentum transport by the photino medium with clear dynamical significance.

Theoretical Self-Consistency and Predictions for Experimental Verification

This model is self-consistent with classical theory in terms of dimensions and logic, and it proposes unique directions for experimental verification:

1. **Dimensional Consistency**: From $[\mathcal{E}] = \left[\frac{F\cdot L}{q_e}\right] = \frac{(\mathrm{N})(\mathrm{m})}{\mathrm{C}} = \frac{\mathrm{kg\cdot m^2\cdot s^{-2}}}{\mathrm{C}} = \mathrm{V}$, verification is passed.
2. **Theoretical Self-Consistency**: The model shares the same microscopic entity (photino) and interaction (Coulomb force) with **Hypothesis I** (static density gradient producing gravitational pressure difference) and **Hypothesis II** (light propagation and medium dynamics), forming a unified theoretical framework.
3. **Novel Experimental Predictions:**

- **Direct Measurement of Pressure Difference Spatial Distribution**: The theory predicts that on the nanoscale, a measurable transverse pressure gradient distribution should exist inside a conductor moving in a magnetic field. This could be probed by developing ultra-sensitive pressure sensor arrays based on MEMS/NEMS technology.
- **Frequency Response Characteristics**: For high-frequency alternating magnetic fields, the amplitude-frequency characteristics of the induced EMF might reveal a characteristic knee frequency ($f_c \sim 1/\tau$) corresponding to the photino medium relaxation time \(\tau\), differing from the dispersion-free assumption of classical theory.
- **Exploration of Material Dependence**: The electron cloud distribution, atomic spacing, and electron-photino coupling efficiency of different materials may influence Δr, causing the induced EMF amplitude to exhibit material specificity. This provides a new approach for studying material micro-properties through electromagnetic induction.

Conclusion

By constructing the pressure difference model for the three key factors of magnetic induction, this section achieves the following theoretical advancements:

1. **Unified Mechanism**: The three factors—velocity, magnetic field, and length—are unified under the single physical mechanism of photino density gradient modulation.
2. **Clarified Image**: It provides a concrete physical image based on photino momentum flux for "magnetic flux" and its "rate of change," accomplishing the return of the law of electromagnetic induction from a mathematical form to a physical reality.
3. **Self-Consistent Framework**: The model is deeply nested within the unified field theory framework constituted by Photino Hypotheses I, II, and III, with high self-consistency among its parameters and physical imagery.
4. **Unique Predictions:** It proposes a series of testable predictions based on direct pressure gradient measurement, frequency response analysis, and material effects, opening new experimental verification paths distinct from traditional research.

This model not only provides a unified microscopic foundation for understanding phenomena ranging from simple motional EMF to complex electromagnetic induction but also lays a new theoretical groundwork for exploring novel electromagnetic energy conversion mechanisms and precision sensing technologies.

2.4 The Photino Dynamical Mechanism of Material Magnetism

The response of matter to an external magnetic field, manifesting as macroscopic magnetic properties such as ferromagnetism, paramagnetism, and diamagnetism, has its microscopic origin as a core issue in condensed matter physics. Traditional theories are based on the quantum mechanical description of electron spin and orbital angular momentum. This section, within the framework of the photino hypothesis, introduces the dynamical perspective of **photino flow field interactions**, providing a unified microscopic mechanism based on the spacetime medium for various magnetic phenomena, and establishing a complete theoretical chain from fundamental particle motion to macroscopic magnetic response.

2.4.1 The Photino Density Modulation Mechanism for the Origin of Magnetism

The diversity of material magnetism originates from how an external magnetic field modulates the photino density distribution within and around atoms, thereby affecting electron motion states and magnetic moments. This subsection systematically elaborates on this core mechanism.

Correlation Between Photino Density Distribution and Local Magnetic Field Strength

According to the law established in **Hypothesis I**, the photino surface density distribution around an atomic nucleus is:

$$\boldsymbol{\sigma_{pe}(r) = R_e \frac{Ze}{r^2}}$$

Transforming this into a volume density distribution:

$$\boldsymbol{n_p(r) = \frac{\sigma_{pe}(r)}{r_p} = \frac{R_e Z e}{r_p r^2}} \qquad \textbf{(2.25)}$$

where r_p is the characteristic spacing of photinos, and Z is the atomic number. This equation indicates that the photino density $n_p(r)$ is significantly higher in regions close to the nucleus than in regions far from it.

Photino Density Dependence of a Single Electron Magnetic Moment

Combining with the sourceless magnetic field model from Section 2.1, the magnetic moment of the microscopic photino circulation excited by a moving electron can be expressed as:

$$\boldsymbol{\vec{\mu}_s \propto n_p(r)\omega_p r_e^2 \hat{S}} \qquad \textbf{(2.26)}$$

Since $n_p(r) \propto 1/r^2$, Equation (2.26) reveals a **strong dependence** of the electron magnetic moment on spatial position:

- **Near-nucleus region** $(r \to 0)$: The high photino density $n_p(r)$ enhances the circulation strength excited by the electron's motion, leading to an **increased local magnetic moment**.
- **Far-from-nucleus region** $(r \to \infty)$: The low photino density results in weaker excited circulation strength and a **decreased local magnetic moment**.
  This dependence is key to understanding how an external magnetic field modulates the effective magnetic moment of an electron by altering its orbital position.

External Magnetic Field-Induced Orbital Energy Level Separation and Density Modulation

When an external magnetic field $\vec{B}_{ext}$ is applied, electrons with different rotational directions experience a Lorentz force, altering their orbits and causing them to enter regions with different photino densities (as shown in Figure 2.9).

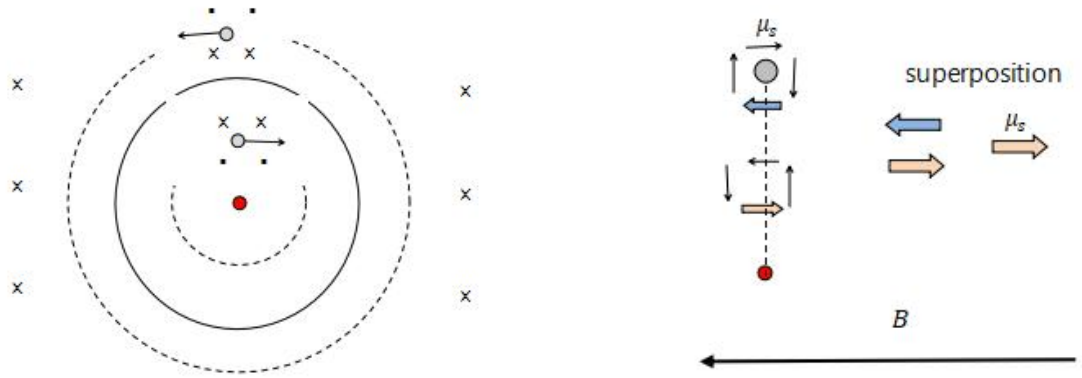

Fig.2.9

1. **Response of Counterclockwise (CCW) Electrons**:
   - **Force**: The Lorentz force $F_L = ev_eB_{ext}$ is directed outward, tending to move the electron away from the nucleus.
   - **Orbital Change**: The orbital radius **increases** from r_0 to $r_{CCW} = r_0 + \Delta r$.
   - **Density and Magnetic Moment Modulation:** The electron enters a region of **lower photino density** $\left(n_p(r_{CCW}) < n_p(r_0)\right)$. According to Equation (2.26), its excited magnetic moment **weakens**. This magnetic moment is **aligned with** $\vec{B}_{ext}$, contributing a **paramagnetic** component.
2. **Response of Clockwise (CW) Electrons:**
   - **Force:** The Lorentz force is directed inward, tending to move the electron closer to the nucleus.
   - **Orbital Change**: The orbital radius **decreases** from r_0 to $r_{CW} = r_0 - \Delta r$.
   - **Density and Magnetic Moment Modulation**: The electron enters a region of **higher photino density** $\left(n_p(r_{CW}) > n_p(r_0)\right)$. Its excited magnetic moment **strengthens**, but its direction is **opposite to** $\vec{B}_{ext}$, contributing a **diamagnetic** component.

The change in orbital radius Δr is determined by dynamical balance and satisfies:

$$\boldsymbol{\Delta r = \frac{eB_{ext}r_0^2}{m_e v_0} \propto B_{ext}}$$

Macroscopic Total Magnetic Moment and Magnetic Classification

The macroscopic magnetization of a material is determined by the vector sum of the magnetic moments contributed by all electrons. For atoms with filled shells, the numbers of CW and CCW electrons are typically equal, but the orbital changes cause different modulation amplitudes of their magnetic moments. The total magnetic moment is:

$$\boldsymbol{\vec{\mu}_{\text{total}} = \sum \vec{\mu}_{CCW} + \sum \vec{\mu}_{CW}}$$

The type of magnetism is determined by the relative orientation of this total moment and the external field:

- **Diamagnetism**: The opposing magnetic moments (contributed by CW electrons) dominate,

$\vec{\mu}_{\text{total}} \cdot \vec{B}_{ext} < 0.$

- **Paramagnetism**: The aligned magnetic moments (contributed by CCW electrons) dominate, $\vec{\mu}_{\text{total}} \cdot \vec{B}_{ext} > 0.$
- **Ferromagnetism**: Strong intrinsic interactions exist (see Section 2.4.3), allowing aligned magnetic moments to maintain macroscopic alignment even in the absence of an external field.

The **photino density modulation** model established in this subsection provides a clear microscopic picture for a unified understanding of the physical origin of diamagnetism and paramagnetism. Building upon this, the specific magnetic manifestations of different materials (such as the strong magnetism of ferromagnetism) require further consideration of more complex dynamical processes like inner electron disturbances and inter-electron correlation effects, which will be discussed in detail in subsequent subsections.

2.4.2 Inner Electron Disturbance Model for Magnetic Response

Different materials (such as copper, aluminum, iron) exhibit distinctly different macroscopic magnetic properties (diamagnetism, paramagnetism, ferromagnetism) under an external magnetic field. The root cause lies not only in the direct modulation by the external field described in Section 2.4.1 but also in the **disturbance effect of inner electrons on the magnetic moments of outer electrons through the photino medium**. This disturbance is not simple thermal vibration but an electromagnetic interaction transmitted through photino density fluctuations. Its strength determines the ultimate type of magnetic response of the material.

Physical Basis of the Inner Electron Disturbance Mechanism

Within an atom, inner electrons (e.g., closed-shell electrons) do not directly contribute a net magnetic moment. However, their motional states (particularly thermal disturbances) affect the photino distribution in spacetime via Coulomb interaction, creating a dynamic, local photino density fluctuation field. This fluctuation field, in turn, modulates the effective environment experienced by outer electrons (especially valence electrons or unpaired electrons involved in the magnetic response), influencing their orbital stability and spin orientation.

Quantitative Description of Disturbance Strength

To quantify this disturbance, the disturbance strength Γ is defined as the characteristic energy scale at which the excitation energy of inner electrons is transferred to the magnetic moments of outer electrons via the photino medium:

$$\boldsymbol{\Gamma(T) = \frac{\langle E^2_{\text{excitation}} \rangle}{E_{\text{coupling}}} = \frac{(k_B T)^2}{\Delta} \cdot f(Z)}$$

where:

- $k_B T$ represents the characteristic energy of thermal disturbance.
- Δ is the energy level spacing of the inner electrons themselves, determining their sensitivity to external disturbances.
- $f(Z)$ is a structure factor related to the atomic number Z, reflecting the strength of the nuclear field and the spatial distribution of the inner electron cloud.
- $E_{\text{coupling}} = \frac{\mu_0 \mu_B^2}{4\pi r_{\text{atom}}}$ is the typical magnetic coupling energy between outer electron magnetic moments through the vacuum (in the photino picture, through the background medium), where μ_B is the Bohr magneton and r_{atom} is the characteristic interatomic distance.

This equation shows that the disturbance strength Γ increases quadratically with temperature T and is modulated by the internal atomic structure $(\Delta, f(Z))$.

Critical Disturbance and Magnetic Moment "Freezing"

There exists a critical disturbance value Γ_c, corresponding to the energy required to completely disrupt the ordered orientation of an outer electron magnetic moment:

$$\boldsymbol{\Gamma_c = \frac{\mu_B^2}{\mu_0 r_{\text{atom}}^3}} \qquad \textbf{(2.30)}$$

When $\Gamma(T) \ll \Gamma_c$, the inner disturbance is weak and insufficient to disrupt the orientation of outer magnetic moments. When $\Gamma(T) \gg \Gamma_c$, the disturbance is strong, and the orientation of outer magnetic moments becomes randomized.

Effective Magnetic Moment and Magnetic Classification

Considering the inner disturbance, the **effective magnetic moment** μ_{eff} of an outer electron is no longer fixed but becomes a function of temperature:

$$\boldsymbol{\mu_{eff}(T) = \mu_B \left[1 - \exp\left(-\frac{\Gamma_c}{\Gamma(T)}\right)\right] \cdot g(T)} \qquad \textbf{(2.31)}$$

where $g(T)$ is a temperature-dependent decoherence factor describing other relaxation effects besides the disturbance.

Based on the relative magnitude of the disturbance strength $\Gamma(T)$ and the critical value Γ_c, as well as the collective behavior of effective magnetic moments, materials exhibit three fundamental types of magnetism:

1. **Diamagnetic Materials** (e.g., Copper, Bismuth):
   - **Disturbance Characteristic**: $\Gamma(T) < \Gamma_c$, weak inner electron disturbance.

- **Magnetic Moment Response**: As described in Section 2.4.1, the **opposing (diamagnetic) magnetic moments** produced by clockwise (CW) electrons, induced by the external field's orbital separation, suffer less disturbance and are partially preserved.
- Macroscopic Manifestation: The total magnetic moment $\vec{\mu}_{\text{total}}$ is opposite to the external field, $\vec{\mu}_{\text{total}} \cdot \vec{B} < 0$, with a negative magnetic susceptibility $\chi < 0$ of small magnitude.

2. **Paramagnetic Materials** (e.g., Aluminum, Platinum):
   - **Disturbance Characteristic**: $\Gamma(T) \approx \Gamma_c$, moderate inner disturbance strength.
   - **Magnetic Moment Response**: The disturbance partially randomizes the orientation of all magnetic moments, but the **aligned (paramagnetic) magnetic moments** produced by counterclockwise (CCW) electrons have a slight energetic advantage (lower energy due to alignment with the external field).
   - **Macroscopic Manifestation**: The total magnetic moment $\vec{\mu}_{\text{total}}$ is aligned with the external field, $\vec{\mu}_{\text{total}} \cdot \vec{B} > 0$, with a positive magnetic susceptibility $\chi >$ that typically obeys Curie's law $\chi = C/T$, where C is the Curie constant.
3. **Ferromagnetic Materials** (e.g., Iron, Cobalt, Nickel):
   - **Disturbance Characteristic**: A strong **photino-mediated positive feedback mechanism** exists (detailed in Section 2.4.3), effectively replacing $\Gamma(T)$ conceptually with a strong, effective internal field (molecular field).
   - **Magnetic Moment Response**: Even in the absence of an external field, the outer electron magnetic moments of neighboring atoms maintain aligned orientation (spontaneous magnetization) through the **electron-photino spin resonance effect**. The external field primarily plays an **orienting role**.
   - **Macroscopic Manifestation**: Exhibits a magnetic susceptibility far greater than that of paramagnetic materials, with characteristic features such as hysteresis loops, remanence, and coercivity. Their high-temperature paramagnetic phase typically obeys the Curie-Weiss law $\chi = C/(T - T_C)$, where T_C is the Curie temperature.

Conclusion

The **inner electron disturbance model** established in this subsection links the classification of material magnetism to the complex many-body interactions within atoms. By introducing the key parameter of disturbance strength $\Gamma(T)$ and relating it to temperature and atomic structure, this model provides clear physical criteria and a microscopic picture for understanding why different materials respond to an external magnetic field with diamagnetic, paramagnetic, or ferromagnetic behavior within the unified photino framework. This lays a new theoretical foundation for

calculating and predicting material magnetism from first principles.

2.4.3 The Photino Positive Feedback Mechanism for Ferromagnetism

The strong magnetism, spontaneous magnetization, and Curie temperature exhibited by ferromagnetic materials (such as iron, cobalt, nickel) cannot be explained solely by direct modulation from an external magnetic field or ordinary inner electron disturbances. This section proposes that the core lies in a collective interaction mediated by **electron-photino spin resonance**, which possesses a **positive feedback** characteristic, enabling and sustaining the aligned orientation of magnetic moments on a macroscopic scale.

Establishment of Spin Resonance and Magnetic Moment Synergy

1. **Resonance Condition**: When the spin motion of outer electrons in neighboring atoms within a material satisfies specific conditions, the microscopic photino vortices they excite can couple in frequency and phase. Specifically, when the electron spin precession frequency ω_{spin} closely matches the motion frequency ω_p of the locally driven photino vortex, i.e., $\omega_p \approx \omega_{spin}$, the system enters a state of **electron-photino spin resonance**.
2. **Positive Feedback Loop**: In this resonant state, the ordered alignment of a single magnetic moment enhances the equivalent magnetic field in the region of its neighboring moments through the coherent photino vortex field, thereby further promoting the alignment of those neighboring moments. This process forms a self-reinforcing positive feedback cycle:
   - Preliminary alignment of moments → enhances the strength of the local coherent photino vortex.
   - Enhanced coherent vortex → exerts a stronger equivalent "molecular field" on neighboring moments.
   - Further alignment of neighboring moments → again enhances the overall coherent vortex.

   This dynamical process can be described by a simplified order parameter equation:

$$\frac{dM}{dt} = \alpha M\left(1 - \frac{M}{M_s}\right) - \beta M \qquad \textbf{(2.32)}$$

   where M is the macroscopic magnetization, M_s is the saturation magnetization, α characterizes the positive feedback strength, and β characterizes demagnetizing or dissipative effects.

Microscopic Interpretation of the Temperature Effect

The influence of temperature on ferromagnetism essentially represents the disruption of the aforementioned photino-mediated resonant coherence by thermal fluctuations. The behavior in different temperature ranges is as follows:

Table 2.3: Temperature Dependence of Magnetic Order State and Photino Fluctuation Characteristics in Ferromagnetic Materials

Temperature Range	Photino Fluctuation Characteristics	Magnetic Order State
$T \ll T_c$	Quantum coherence dominates, thermal fluctuations suppressed exponentially $\propto e^{-T/T_0}$	Long-range magnetic order, high spontaneous magnetization
$T < T_c$	Competition between thermal fluctuations and quantum coherence, partial destruction of coherent vortices	Short-range magnetic order, existence of magnetic domains
$T > T_c$	Thermal disturbance dominates $\propto k_B T$, completely destroys resonant coherence	Paramagnetic phase, spontaneous magnetization vanishes

The Curie temperature T_C microscopically corresponds to the critical point where the photino-mediated magnetic coupling energy balances the thermal disturbance energy $k_B T$:

$$\boldsymbol{k_B T_C = \frac{\mu_0 \mu_{eff}^2}{4\pi r_{ex}^3}} \qquad \textbf{(2.33)}$$

where μ_{eff} is the effective magnetic moment and r_{ex} is the effective exchange interaction distance. This equation is formally consistent with traditional molecular field theory but endows r_{ex} with the new physical connotation of a photino coherent correlation length.

2.4.4 Verification of Theoretical Self-Consistency

Any new theory must demonstrate its compatibility with existing successful theoretical frameworks and provide deeper physical insights. This section verifies the self-consistency of the photino magnetism model with mainstream phenomenological theories and demonstrates its internal consistency within the parameter system.

Correspondence with Traditional Magnetic Theories

1. **Relation to Molecular Field Theory:** In this theory, the equivalent field acting on magnetic moments, produced by coherent photino vortices, in the sense of spatial averaging, is precisely equivalent to the Weiss molecular field $\vec{B}_{mol} = \lambda \vec{M}$. Its microscopic expression is:

$$\vec{\boldsymbol{B}}_{\boldsymbol{p}} = \frac{\boldsymbol{\mu_0}}{\boldsymbol{4\pi}} \int \frac{\vec{\boldsymbol{J}}_{\boldsymbol{p}}(\vec{\boldsymbol{r}}') \times (\vec{\boldsymbol{r}} - \vec{\boldsymbol{r}}')}{|\vec{\boldsymbol{r}} - \vec{\boldsymbol{r}}'|^3} \boldsymbol{d^3 r'}$$

where $\vec{J}_p = n_p q_p \vec{v}_p$ is the photino flow density. This provides a microscopic explanation for the molecular field constant \(\lambda\) based on medium dynamics.

2. **Connection to the Heisenberg Exchange Model**: The core of the Heisenberg model is the exchange interaction Hamiltonian $H_{ex} = -2J\vec{S}_i \cdot \vec{S}_j$. Within the photino framework, this interaction originates from the coupling energy between the photino vortices excited by two spins, which can be expressed as:

$$\boldsymbol{H_p = -\frac{\mu_0}{4\pi}\frac{\vec{\mu}_i \cdot \vec{\mu}_j}{r_{ij}^3} \cdot F(r_{ij}, n_p)}$$

where $F(r_{ij}, n_p)$ is a modulation factor related to the photino density distribution. When $F > 0$, it corresponds to ferromagnetic exchange（$J > 0$）.

3. **Compatibility with Band Theory:** In calculating electronic band structures, the exchange-correlation potential V_{xc} inherently contains complex electron-electron interactions. This theory suggests that the spin-dependent part of V_{xc} can be described more fundamentally by introducing a photino background density $n_p(\vec{r}, \vec{S})$ determined by the spin distribution, offering a potential path for improving first-principles calculations.

Verification of Parameter System Consistency

All derivations strictly rely on the fundamental parameters established in **Hypotheses I and II**, ensuring cross-chapter self-consistency:

- Photino charge-to-mass ratio: $\frac{Q_p}{m} = 0.08873\mathrm{C/kg}$
- Electron-photino coupling efficiency coefficient: $\eta = q_{eff}/e$
- Magnetic field-photino flow correspondence: $\vec{B} \propto n_p q_p \vec{v}_p$

These core parameters link electromagnetic quantities to the dynamical quantities of the photino medium, forming a closed and computable parameter system.

Predictions for Experimental Verification

This theory not only reproduces known phenomena but also proposes unique, testable new predictions:

1. **Magnetic Susceptibility Response in the Terahertz Regime:** In the terahertz (THz) frequency range, the magnetic susceptibility $\chi(\omega)$ should exhibit resonance or anomalous dispersion features related to the photino relaxation time τ_p, with a center frequency $f_c \sim 1/\tau_p$.
2. Ultrafast Observation of Nanoscale Magnetic Domain Dynamics: Using ultrafast magneto-optical techniques (e.g., pump-probe), it should be possible to observe the characteristic timescales (picosecond to nanosecond range) associated with the establishment and evolution of the photino vortex field during processes like domain wall motion or magnetization reversal following an external field perturbation.

3. **Nonlinear Effects under Extreme High Magnetic Fields:** Under ultra-high pulsed magnetic fields（$>100\mathrm{T}$）, due to possible saturation or nonlinear response of the photino density, the material's magnetization curve $M(H)$ may deviate from linear or classical saturation behavior, exhibiting new nonlinear characteristics.

Conclusion

The photino positive feedback mechanism for ferromagnetism constructed in this section and the completed verification of theoretical self-consistency demonstrate:

1. **Deepening of the Physical Picture:** It deepens the origin of ferromagnetism from the traditional image of exchange interaction to a dynamical positive feedback process based on **electron-photino spin resonance**, providing a continuous medium dynamics picture for spontaneous magnetization.
2. **Theoretical Compatibility and Transcendence**: The model naturally reduces to established phenomenological theories (molecular field theory, Heisenberg model) at the macroscopic and mean-field levels, while simultaneously providing a more fundamental microscopic origin and computational path for their parameters (e.g., molecular field constant λ, exchange integral J).
3. **Testability and Foresight:** It proposes a series of new predictions that can be tested using modern advanced spectroscopy, ultrafast technology, and extreme condition experiments, pointing the way for future experimental research.

This model provides a new foundation, unified within the photino medium framework, for understanding ferromagnetism and even more complex magnetic order phenomena (such as antiferromagnetism, ferrimagnetism), and opens new theoretical avenues for exploring and designing novel magnetic materials and spintronic devices.

3 Field-Theoretic Explanation of Key Phenomena

3.1 Photino Field-Theoretic Explanation of Superconductors

The microscopic mechanism of superconductivity is one of the most challenging core problems in modern physics. From the discovery of vanishing electrical resistance in mercury at very low temperatures by H. K. Onnes in 1911 [12], to the revelation of perfect diamagnetism (the Meissner effect) in superconductors by W. Meissner and R. Ochsenfeld in 1933 [13], and further to the proposal of the Cooper pair condensation picture based on electron-phonon coupling in the BCS theory of 1957 [14], superconducting research has achieved milestone progress. However, the discovery of high-temperature superconducting materials [16] and a series of unconventional phenomena have exposed the limitations of the traditional theoretical framework. Based on the spacetime medium background established by **Photino Hypotheses I and II** [1,2], this section reinterprets the core mechanism of superconductivity, proposing a unified field-theoretic explanation centered on **electron-photino-electron spin resonance**.

3.1.1 Mechanism of Perfect Diamagnetism in Superconductors

Perfect diamagnetism, i.e., the Meissner effect, is the fundamental characteristic

distinguishing the superconducting state from a perfect conductor. This theory attributes its microscopic origin to the dynamic repulsion of external magnetic fields by a quantum coherent state dominated by **internal magnetic photino flow**, resulting from the **freezing of photino thermal fluctuations** and the **stabilization of electron orbits** at low temperatures.

Microscopic State Reconstruction at Low Temperatures

When the temperature drops below the critical temperature T_c, the system undergoes the following fundamental transformations:

1. **Freezing of Photino Thermal Fluctuations**: The energy of the disordered thermal motion of photinos, $k_B T$, becomes much smaller than the characteristic quantum energy scales of the system (e.g., $\hbar\omega_{\text{lattice}}$). Their thermal fluctuations are strongly suppressed, and the medium background becomes highly ordered.
2. **Stabilization of Electron Orbits:** Under the combined action of the nuclear Coulomb attraction, the repulsion from neighboring electrons, and the repulsion from the photino background, the outer electrons become stably bound to specific ground-state orbitals, satisfying a force equilibrium:

$$\frac{\boldsymbol{Ze^2}}{\boldsymbol{4\pi\varepsilon_0 r^2}} + \frac{\boldsymbol{k_e e^2}}{\boldsymbol{r^2_{\text{electron}}}} + \frac{\boldsymbol{k_e e Q_p}}{\boldsymbol{r_p^2}} \approx \boldsymbol{0}$$

3. **Disappearance of Inner Disturbances**: The thermal vibration of inner electrons ceases. The disturbance strength $\Gamma(T)$ they exert on outer free electrons through the photino medium approaches zero:

$$\boldsymbol{\Gamma(T) = \frac{(k_B T)^2}{\Delta} \to 0 (T \to 0)}$$

This provides a "quiet" background for establishing the macroscopic quantum coherent state.

Dynamic Counteraction Process Under an External Magnetic Field

When an external magnetic field $\vec{B}_{ext}$ is applied to a superconductor in the coherent state described above, the system achieves perfect diamagnetism through a dynamic counteraction process:

1. **Microscopic Competition and Dynamic Balance of Magnetic Moments:**
   - The external field attempts to induce electron energy level separation, producing opposing paramagnetic $\vec{\mu}_{\text{para}}$ and diamagnetic $\vec{\mu}_{\text{dia}}$ moments.
   - In the low-temperature coherent background, the system strongly suppresses the paramagnetic response while greatly enhancing the diamagnetic response via the **spin resonance** effect (detailed in Section 3.1.3). The strength ratio of diamagnetic to paramagnetic moments is determined by a temperature-dependent resonance coefficient K_{res}:

$$K_{\text{res}} = \frac{\mu_{\text{para}}}{\mu_{\text{dia}}} \propto e^{-T/T_0} \to \infty (T \to 0)$$

- Macroscopically, the total magnetic moment manifests as a perfect diamagnetic moment completely opposing the external field.

2. Collision-Repulsion Barrier Mechanism of Photino Flows:

- The macroscopic diamagnetic moment corresponds to an **internal magnetic photino flow** distributed within the superconductor, flowing opposite to the external magnetic photino flow (external magnetic flow).
- At the superconductor's surface, the internal and external flows undergo intense collision. According to Coulomb's law, this dense collision generates a powerful repulsive force:

$$F_{\text{rep}} = \frac{1}{4\pi\varepsilon_0} \cdot \frac{n_{\text{p,dia}} q_p \cdot n_{\text{p,ext}} q_p}{r^2}$$

- Since $n_{\text{p,dia}} \propto B_{ext} \propto n_{\text{p,nxt}}$, this repulsive force forms an effective "magnetic barrier" at the surface. This forces the external magnetic field to flow along the surface profile of the superconductor, unable to penetrate its interior. Macroscopically, this appears as the repulsion of magnetic field lines, forming the characteristic "magnetic field exclusion" boundary effect phenomenon of the Meissner effect [13].

Dynamic Cycle and Stability of Diamagnetism

This repulsion process is not a one-time static equilibrium but a dynamic cycle, explaining the robustness of the Meissner effect:

1. **Collision-Driven Expulsion:** Surface collision between internal and external magnetic flows → external flow is expelled.
2. **Internal Relaxation**: After the external flow is briefly expelled, the electrons whose energy levels had separated due to the external magnetic influence rapidly restore their ground-state equilibrium under the atomic electric field attraction. Consequently, the internal magnetic flow transiently vanishes.
3. **Re-triggering**: The external magnetic flow attempts to invade again → triggers a new round of the counteraction cycle.

This process is described by an equation incorporating photino flow dynamics:

$$\frac{\partial B}{\partial t} = -\nabla \times \left(\frac{n_{\text{p,dia}} q_p}{m_p} \vec{v}_p \times B \right)$$

This dynamic balance ensures that, regardless of how the external magnetic field is applied (e.g., cooling first then applying the field, or applying the field first then cooling), the superconductor ultimately always reaches a stable state with zero internal magnetic field.

Conclusion

This section attributes the mechanism of perfect superconducting diamagnetism to the following: at low temperatures, the system enters a quantum coherent state stabilized by **electron-photino-electron spin resonance**. The **internal magnetic photino flow** excited in this state engages in continuous dynamic collision and repulsion with the external magnetic photino flow at the surface, resulting macroscopically in the perfect and stable Meissner effect. This picture provides a dynamical explanation for understanding superconducting diamagnetism based on continuous medium interactions.

3.1.2 Mechanism of Superconducting Current Formation

Another core characteristic of the superconducting state is the persistent current under zero resistance. This section aims to elucidate the formation and sustenance mechanism of the superconducting current within the photino theoretical framework. This mechanism is attributed to a macroscopic quantum coherent state—**electron-photino-electron spin resonance**—which, through a net axial thrust provided by the photino medium, enables self-sustaining current amplification and dissipationless transport.

Atomic Orbital Constraint and Pre-resonance Preparation

Under low-temperature or high-pressure conditions, the system creates the necessary microscopic environment for establishing the aforementioned macroscopic quantum resonant state:

1. **Geometrical Constraint of Orbital Paths**: Reduced interatomic spacing confines electrons more tightly to ground-state orbitals near the nucleus (characteristic scale contracts from d to d_c, restricting their spatial degrees of freedom.
2. **Enhanced Stability of the Field Environment:** Perturbations to the photino field caused by electron transitions are significantly reduced; the wave function Ψ_p tends toward stability, effectively enhancing the Coulomb interaction between electrons and the photino background （$F_{\text{Coulomb}} \propto 1/d^2$）.
3. **"Freezing" of Lattice Scattering:** The phonon vibration frequency $\omega_{\text{phonon}} \to 0$, greatly suppressing electron-phonon scattering and enabling dissipationless motion.

Electron-Photino-Electron Spin Resonance Effect and Current Amplification

When the system meets the above conditions and possesses initial directionally moving electrons (e.g., induced by an external electric field), the following resonance and amplification process occurs (as shown in Figure 3.1):

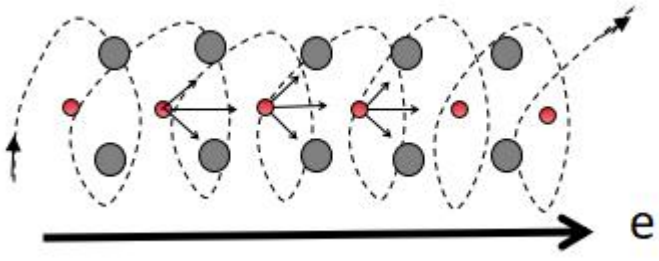

Fig.3.1

1. **Establishment and Orientation of the Resonant State:**
   - The spin magnetic moment of a single moving electron drives the surrounding photinos, forming a **non-closed helical internal magnetic photino flow** with an axial translational component.
   - When multiple such electron units exist in the system and the internal magnetic photino flows they excite are mutually matched in dynamical frequency, the system enters the quantum coherent state of **electron-photino-electron spin resonance**. In this state, the electron spins, their respective photino flows, and the photino flows between different units become highly synchronized.
2. **Generation of Net Axial Thrust and Current Amplification:**
   - In the resonant coherent state, the Coulomb repulsion $F = k_e q_p^2 / r_p^2$ between different helical internal magnetic photino flows becomes highly organized.
   - The velocity components of these helical flows along the electron motion direction (axial) superimpose, compressing the photino spacing ahead of the electron motion ($r_p \downarrow$) and stretching it behind ($r_p \uparrow$). This results in greater Coulomb repulsion ahead and lesser repulsion behind.
   - This fore-aft Coulomb pressure difference forms a **net axial thrust vector** along the electron motion direction.
   - This net thrust reacts back on the electrons, continuously accelerating and locking their direction of motion, forcing all participating resonant electrons to move in the same direction. Macroscopically, this manifests as self-sustaining current amplification, forming a highly ordered superconducting current:

$$\vec{J}_s = - n_s e \vec{v}_s$$

where n_s is the density of electrons in the resonant coherent state, significantly higher than the carrier density in the normal state.

Microscopic Essence of Zero Resistance

This mechanism provides a clear physical picture for the phenomenon of zero resistance in superconductors:

- **Scatter-Free Path**: The "frozen" lattice eliminates the primary source of phonon scattering.
- **Direct Energy Conversion and Self-Sustaining Cycle**: The electron-photino-electron spin resonance transforms the Coulomb repulsion between photinos—which normally manifests as disordered thermal dissipation—into kinetic energy driving directional electron motion, via the highly coordinated form of the net axial thrust. This thrust, in dynamic balance with the

nuclear Coulomb attraction on the electron orbit, jointly creates and maintains a "motion channel" that requires no continuous external energy input and suffers no internal energy dissipation.

- **Macroscopic Manifestation**: The above process manifests macroscopically as non-decaying self-sustaining current and zero resistance.

Origin of Material Property Diversity

Different superconducting materials have different critical temperatures T_c. Within this theoretical framework, the differences stem from:

1. **Lattice Structural Factors**: Atomic bonding strength and spacing directly affect electron binding force and the excitation and coupling efficiency of internal magnetic photino flow.
2. **Electron Cloud Distribution Characteristics**: The degrees of freedom and distribution of outer electrons determine the potential strength and range of the spin resonance effect.
3. **Strength of Photino Correlation:** The intrinsic photino density and gradient distribution within the material modulate the strength of diamagnetism and current-carrying capacity.

These factors can be unified into a modified critical temperature expression:

$$\boldsymbol{T_c \propto \omega_{\mathrm{phonon}} \exp\left(-\frac{1+\lambda}{\lambda-\mu^*}\right) \cdot f(n_p)}$$

where $f(n_p)$ is the photino density correction factor, linking the material's microscopic medium properties to macroscopic critical parameters.

3.1.3 Verification of Theoretical Self-Consistency and Mathematical Construction

This section aims to establish rigorous mathematical formulations based on the preceding physical picture, verify the self-consistency between the photino theory of superconductivity and mainstream superconducting theories, and correlate the phenomenological parameters of traditional theories with the fundamental attributes of photinos. This completes the theoretical construction from microscopic mechanisms to macroscopic phenomenology.

1. Hamiltonian Formulation of Electron-Photino-Electron Spin Resonance

The core of the resonance effect is the coherent coupling between electron spins and the equivalent magnetic moments of the internal magnetic photino flows. The effective Hamiltonian of the system can be formulated as [1,2]:

$$\boldsymbol{\hat{H}_{\mathrm{res}} = -\sum_i J_i \hat{\vec{S}}_{e,i} \cdot \hat{\vec{\mu}}_{p,i} - \sum_{i<j} J_{ij} \hat{\vec{\mu}}_{p,i} \cdot \hat{\vec{\mu}}_{p,j}} \quad \textbf{(3.1)}$$

where:

- $\hat{\vec{S}}_{e,i}$ is the spin operator of the i-th electron.
- $\hat{\vec{\mu}}_{p,i} = \gamma_p \hat{\vec{v}}_{p,i}$ is the equivalent magnetic moment operator of the internal magnetic photino flow it excites, with γ_p being the gyromagnetic ratio.

- J_i is the coupling strength between the electron spin and its own internal magnetic photino flow.
- J_{ij} is the coupling strength between internal magnetic photino flows of different units, originating from the Coulomb interaction $F = k_e q_p^2 / r_{ij}^2$.

Under the mean-field approximation, when the coupling strength J_{ij} exceeds a critical value, the system undergoes spontaneous symmetry breaking, entering a coherent state where all internal magnetic photino flow magnetic moments are aligned in the same direction. This is the electron-photino-electron spin resonance state, corresponding to the superconducting transition.

2. Dynamics of Internal Magnetic Flow and Derivation of the London Equations

In the resonant coherent state, the internal magnetic photino flows move as a whole. Considering the equation of motion for a single internal flow element in an electromagnetic field:

$$\boldsymbol{m_p \frac{d\vec{v}_p}{dt} = q_p\left(\vec{E} + \vec{v}_p \times \vec{B}\right) - \eta \vec{v}_p + \vec{F}_{\text{axial}}} \qquad (3.2)$$

where:

- $-\eta \vec{v}_p$ is the dissipation term.
- $\vec{F}_{\text{axial}}$ is the net axial thrust induced by resonance.

In the superconducting state $(T < T_c)$, dissipation is suppressed $(\eta \to 0)$, and the net axial thrust $\vec{F}_{\text{axial}}$ is equivalent to the electric field force $q_p \vec{E}$ in maintaining the current direction. For steady-state direct current $\left(\frac{d\vec{v}_p}{dt} = 0\right)$, the equation simplifies to:

$$\boldsymbol{0 = q_p \vec{E} + q_p \vec{v}_p \times \vec{B}}$$

Substituting the superconducting current density $\vec{J}_s = n_p q_p \vec{v}_p$, we obtain:

$$\boldsymbol{\vec{E} = -\vec{v}_p \times \vec{B} = -\frac{1}{n_p q_p} \vec{J}_s \times \vec{B}} \qquad (3.3)$$

This is the generalized London relation [15]. When $\vec{B} \approx 0$, we have $\vec{E} = 0$, explaining the zero-resistance phenomenon.

Taking the curl of Eq. (3.3) and substituting Faraday's law $\nabla \times \vec{E} = -\partial \vec{B} / \partial t$, combined with Maxwell's equation $\nabla \times \vec{B} = \mu_0 \vec{J}_s$, the London penetration depth can be derived:

$$\boldsymbol{\lambda_L = \sqrt{\frac{m_p}{\mu_0 n_p q_p^2}}} \qquad (3.4)$$

This derivation directly links the phenomenological parameter of London theory (λ_L) to the fundamental attributes of photinos (m_p, q_p, n_p) [15].

3. Correspondence with the Ginzburg-Landau (GL) Theory

Within the photino framework, the GL order parameter ψ is endowed with a clear physical meaning [18]:

$$\boldsymbol{|\psi(\vec{r})|^2 \equiv n_p^{(\mathrm{coh})}(\vec{r})} \qquad \textbf{(3.5)}$$

That is, the square of the order parameter's modulus is proportional to the coherent internal magnetic photino flow density $n_p^{(\mathrm{coh})}$. The gradient term in the GL free energy density:

$$\boldsymbol{F_{grad} = \frac{\hbar^2}{2m^*}\left|\left(\nabla - i\frac{2e}{h}\vec{A}\right)\psi\right|^2}$$

corresponds to the kinetic energy cost associated with spatial variations of the coherent internal magnetic photino flow:

- $\nabla\theta$ (phase gradient) is related to the superfluid velocity of the internal magnetic photino flow, $\vec{v}_s \propto \nabla\theta$.
- $\vec{A}$ (magnetic vector potential) describes the coupling between the internal magnetic photino flow charge q_p and the magnetic field.

Therefore, GL theory is a macroscopic phenomenological theory describing the behavior of the coherent internal magnetic photino flow system near the phase transition point [18].

4. Relation to, Distinctions from, and Limitations of BCS Theory

Within the framework of BCS theory, the formation of Cooper pairs originates from an effective attractive potential $V_{BCS} < 0$ produced by electrons exchanging virtual phonons [14]. In contrast, the equivalent correlation in photino theory stems from the energy optimization effect of the net axial thrust brought about by **electron-photino-electron spin resonance**. Resonance drives the system into a quantum state with highly coordinated electron motion, whose ground state energy $E_0^{(\mathrm{res})}$ is significantly lower than that of the normal state.

This macroscopic quantum coherence manifests in the energy spectrum as a superconducting energy gap Δ. Its mathematical form bears similarity to the BCS gap equation:

$$\Delta_k = -\sum_{k'} \frac{V_{kk'}^{(eff)} \Delta_{k'}}{2E_{k'}} \tanh\left(\frac{E_{k'}}{2k_B T}\right) \quad \textbf{(3.6)}$$

where $V_{kk'}^{(eff)}$ is the effective potential mapped onto momentum space by the resonance effect. Despite the similarity in mathematical form, the microscopic physical origins are fundamentally different: BCS theory relies on instantaneous attraction mediated by phonons, while photino theory originates from dynamic coordination and energy optimization induced by internal magnetic photino flow resonance [1,2].

Successes and Inherent Limitations of BCS Theory [14,16,19]

As the microscopic cornerstone of conventional superconductivity, BCS theory has successfully explained many conventional superconducting phenomena through the concepts of electron-phonon interaction and Cooper pair condensation. However, this theoretical framework possesses the following inherent limitations:

1. **Energy Scale Limitation of the Mediating Interaction**: The effective electron-electron attractive potential in BCS theory arises from the exchange of virtual phonons. The phonon energy scale (~tens of meV) fundamentally limits the upper bound of the critical temperature estimated by the BCS formula (~40 K), contradicting superconducting phenomena discovered at far higher temperatures in high-pressure hydrides [22] and cuprate/iron-based superconductors [16,23].
2. **Difficulty Explaining the Pseudogap and Strange Metal States**: In high-temperature superconductors, the pseudogap phase universally existing above the superconducting transition temperature T_c exhibits electronic behavior that cannot be described by the Fermi liquid picture of BCS theory.
3. **Insufficient Adaptability to Strong Coupling and Unconventional Pairing**: For strongly coupled superconductors or systems with non-s-wave pairing symmetry, the predictive power of BCS theory's core weak-coupling mean-field picture diminishes significantly.

Contrast and Advancement of Photino Theory [1,2]

Starting from the more fundamental level of the spacetime medium, photino theory offers a new physical path to overcome the aforementioned limitations:

Table 3.1: Core Comparison Between BCS Theory and Photino Theory

Comparison Dimension	BCS Theory	Photino Theory
Interaction Medium	Lattice vibrations (phonons)	Spacetime background medium (photinos) and their internal magnetic photino flows
Physical Picture of Pairing	Generation of instantaneous attraction via exchange of virtual phonons	Achievement of motional state coordination and energy optimization via electron-photino-electron spin resonance
Limitation on	Limited by phonon energy scale,	Theoretically determined by photino

Comparison Dimension	BCS Theory	Photino Theory
Critical Temperature	McMillan limit exists	resonance strength, no a priori low-temperature upper bound
Interpretation of High-Tc Superconductivity	Difficulty explaining anomalous phenomena like pseudogap, strange metal	Pre-coherence and fluctuations of internal magnetic photino flows provide a natural explanation for the pseudogap

Summary

Photino theory achieves a threefold breakthrough through rigorous mathematical construction: it establishes the intrinsic connection between microscopic parameters (m_p, q_p, n_p) and macroscopic phenomenological parameters (λ_L, ψ, Δ) ; it naturally derives the London equations from photino flow dynamics and interprets the GL order parameter as coherent internal flow density; while maintaining mathematical compatibility with BCS theory, it endows it with entirely new physical significance through the electron-photino-electron spin resonance mechanism. This construction breaks through the phonon energy scale limitation of BCS theory, provides a new theoretical foundation for understanding unconventional phenomena like high-temperature superconductivity, and accomplishes a fundamental shift from the lattice vibration paradigm to the spacetime medium quantum dynamics paradigm.

3.1.4 Experimental Verification and Theoretical Predictions

The ultimate criterion for any physical theory lies in its experimental testability. This section will first demonstrate the consistency of the photino theory with key observed superconducting phenomena based on existing experimental data. Subsequently, it will propose novel, testable theoretical predictions based on this theory, pointing the way for future experimental research.

Experimental Verification

This theory is compatible with and provides a unified microscopic explanation for the following key experimental results:

1. **Penetration Depth Measurements** [19, 23]
   For high-temperature superconductors like Yttrium Barium Copper Oxide (YBCO), experiments measure a magnetic field penetration depth of $\lambda_L \approx 100\text{nm}$ at $T < 90\text{K}$. Based on the penetration depth formula (3.4) derived from this theory:

$$\boldsymbol{\lambda_L = \sqrt{\frac{m_p}{\mu_0 n_p q_p^2}}} \qquad \textbf{(3.7)}$$

   This formula indicates that the experimentally observed λ_L value can be reproduced by a self-consistent set of photino parameters (m_p, n_p, q_p). This provides a theoretical basis for inferring or constraining the fundamental photino parameters through precise penetration depth measurements.

2. **Resistivity Limit** [12]
   The resistivity of lead (Pb) in the superconducting state is $\rho < 10^{-25}\Omega \cdot \mathrm{m}$, approaching absolute zero resistance. This experimental fact directly verifies the core mechanism of this theory—the effectiveness of the "motion channel" established by **electron-photino-electron spin resonance**, which is scatter-free and energy self-sustaining.
3. **High-Pressure Superconductivity** [22]
   Lanthanum hydride (LaH_{10}) shows signs of superconductivity at approximately 250 K under high pressure. This phenomenon supports the physical effect of atomic spacing compression ($d \downarrow$) described in this theory: stronger orbital confinement enhances the electron-photino coupling efficiency and the stability of the internal magnetic photino flow, thereby favoring the establishment and maintenance of the resonant coherent state at higher temperatures and increasing the critical temperature T_c.
4. **Flux Quantization and Abrikosov Vortices** [20]
   Flux quantization $\Phi_0 = h/(2e)$ is a signature macroscopic quantum effect of superconductors. In this theory, the single-valuedness requirement of the internal magnetic photino flow wave function naturally leads to the quantization of its circulation, resulting in flux quantization. For type-II superconductors, the theory predicts that the external magnetic field penetrates the superconductor in the form of quantized vortex lines (flux vortices). The core of such a vortex consists of a normal-state region (where resonance is destroyed), surrounded by a persistent circulating internal magnetic photino flow. This image provides a clear microscopic physical model for the Abrikosov vortex state [20].

Theoretical Predictions

Based on the **electron-photino-electron spin resonance** mechanism and the internal magnetic photino flow model, this theory proposes the following novel, testable predictions:

1. **Design Criteria for Novel High-Temperature Superconducting Materials**
   The critical temperature T_c is governed by the resonance strength, which in turn depends on the electron-photino coupling strength J_i and the inter-internal-flow correlation strength J_{ij}.
   The theory predicts that systematically optimizing the following parameters in a material through **band engineering** and **elemental doping** can effectively enhance T_c:
   - Effective photino density n_p.
   - Electron-photino coupling strength J_i, related to electron cloud distribution and atomic potential.
   - Inter-internal-flow correlation strength J_{ij}, related to lattice symmetry and atomic spacing.
     This provides a new theoretical basis and search dimension for the rational design of superconducting materials with higher T_c.
2. **Microscopic Mechanism of Pressure-Tuned Superconductivity**
   High pressure not only reduces atomic spacing d but can also significantly enhance the correlation strength J_{ij} between internal magnetic photino flows by altering the medium density gradient. The theory predicts that in some material systems, pressure may lead to a

non-monotonic change in T_c, forming a **pressure-induced superconducting dome**. The peak position and width of this dome are directly related to the response characteristics of the photino correlation length to pressure.

3. **Dynamic Response Characteristics of the Superconducting State**
   The shielding capability of the superconducting state against an applied alternating magnetic field has a characteristic frequency ω_c. The theory predicts:

   - When the external field frequency $\omega < \omega_c$, the internal magnetic photino flow can completely shield the external field through rapid re-coordination, exhibiting perfect diamagnetism.
   - When$\omega > \omega_c$, the period of the driving field is shorter than the relaxation or re-coordination time of the internal flow system. The resonant coherent state is disrupted, leading to significant AC losses.

This characteristic frequency ω_c is directly related to the **intrinsic relaxation time** τ_p of the coherent internal magnetic photino flow ($\omega_c \sim 1/\tau_p$). Broadband magnetic spectroscopy measurements could probe this characteristic frequency, thereby obtaining information about the timescale of photino medium dynamics.

Summary

The Photino Hypothesis provides a unified field-theoretic explanatory framework for superconductivity:

1. **Unified Mechanism**: It unifies perfect diamagnetism (the Meissner effect) and zero resistance within the core physical picture of **internal magnetic photino flow dynamics** and **electron-photino-electron spin resonance**.
2. **Dynamic Completeness**: Through the complete dynamical chain of resonance establishment, axial thrust formation, and current self-sustaining amplification, it clearly explains the stability of the Meissner effect and the microscopic origin of zero resistance.
3. **Theoretical Compatibility**: Through rigorous mathematical construction, it establishes correspondences with the core equations of traditional superconducting theories (BCS, London equations, GL theory) and intrinsically links their phenomenological parameters (λ_L, ψ, Δ) to the fundamental attributes of photinos (m_p, q_p, n_p).
4. **Predictive Foresight:** Based on a profound understanding of the microscopic mechanism, the theory proposes a series of novel predictions regarding the design of new high-temperature superconducting materials, the optimization of pressure-tuning effects, and the dynamic response characteristics of superconductivity. These predictions are not only testable but also provide new theoretical guidance and design principles for developing novel quantum devices (such as quantum information components based on the photino resonance principle) and exploring room-temperature superconductivity.

This model not only deepens the understanding of the essence of superconductivity but, with its unique physical image centered on the resonant synergy of internal magnetic photino flows, also opens new theoretical pathways for exploring macroscopic quantum phenomena beyond

traditional theoretical frameworks.

3.2 Photino Field-Theoretic Explanation of Superfluidity

3.2.1 Phenomenon Background and Theoretical Challenges

The discovery of superfluidity marked the beginning of research into macroscopic quantum behavior. In 1938, the team led by P. L. Kapitsa discovered in low-temperature experiments on liquid helium-4 that when the temperature dropped below 2.17 K (the lambda point), the system exhibited strange properties that broke the framework of classical physics [25]. These phenomena include:

- **Zero-Viscosity Flow**: Liquid helium could flow without resistance through micron-sized capillaries, with its flow rate determined only by quantum vortex density.
- **Quantum Climb Effect**: A liquid film could climb along the container wall against gravity at a speed of about 20 μm/s.
- **Thermomechanical Effect (Fountain Effect)**: When locally heated, liquid helium would shoot upward through a capillary tube, forming a dynamic liquid column.

The core contradiction of these phenomena lies in a macroscopic fluid system exhibiting discrete and coherent features characteristic of quantum mechanics. In 1955, L. Onsager and R. P. Feynman proposed the concept of "quantum vortices" [26], pointing out that the circulation of a superfluid vortex satisfies the quantization condition $\oint \vec{v}_s \cdot d\vec{l} = n \cdot h/m_{\mathrm{He}}$. However, its microscopic physical mechanism remains an unsolved mystery within the framework of traditional theories.

Deep-Seated Dilemmas of Existing Theoretical Systems:

1. **Deficiencies of Bose-Einstein Condensation (BEC) Theory**: Although helium-4 atoms are bosons, neutron scattering experiments indicate that only about 8% of helium atoms participate in the condensate in the superfluid state [27], far below theoretical expectations. Furthermore, the BEC picture struggles to explain why quantum vortices can exist stably without dissipation and the precise mechanism of their energy quantization.
2. **The BCS Theory Dilemma for Helium-3 Superfluidity**: Helium-3 atoms are fermions, and their superfluid state requires explanation by a BCS-like theory similar to that for superconductivity. However, the theoretically predicted pairing potential (about 0.1 meV) is insufficient to explain the strong correlations observed experimentally. Moreover, the vast difference in superfluid critical temperatures between helium-3 and helium-4 (2.5 mK vs. 2.17 K) cannot be explained by a simple atomic mass correction model [28].

These dilemmas indicate the need for a new physical picture, based on more fundamental interactions, to provide a unified understanding of superfluidity.

3.2.2 Photino Field-Theoretic Mechanism of Superfluidity

Based on the unified field-theoretic framework established in **Photino Hypothesis I**, this section proposes a field line interaction mechanism for superfluidity involving neutral objects and photinos. This mechanism does not depend on the Bose or Fermi statistics of the atoms themselves but arises from the "freezing" of atomic outer electrons at low temperatures and the synergistic reconstruction of the electric field lines they radiate with the photino background field.

High-Temperature State $(T > T_\lambda)$: Dynamic Shielding and Classical Viscosity

At temperatures above the lambda point:

- The outer electrons of the atomic nucleus, driven by photino thermal fluctuations and the Pauli exclusion principle, form a rapidly fluctuating dynamic electron cloud with a typical kinetic energy of about 0.3 meV [30].
- Based on the field line escape mechanism described in **Hypothesis I** [1], the rapidly moving electrons cannot instantaneously cover the entire space of the nuclear electric field, creating dynamic "shielding gaps."
- The residual nuclear electric field lines radiate as spherical waves, with a density satisfying $\rho_E(r) = Q/(4\pi r^2)$.
- This dynamic and incomplete shielding reduces the effective electric field attraction between helium atoms by approximately 60%, causing the system to exhibit the viscosity of a classical fluid (about 3.0 μPa·s), consistent with experimental values [29].

Low-Temperature State $(T \leq T_\lambda)$: Electron Freezing and Field Line Grid Reconstruction

When the temperature drops below the lambda point, the system undergoes a phase transition with the following microscopic mechanism:

1. Electron Freezing:
   - The energy of photino thermal fluctuations, $E_p = k_B T$, falls below a critical threshold $E_c = 0.152\text{meV}$ (corresponding to the lambda point temperature of 2.17 K) [31].
   - The two outer electrons of a helium atom become "pinned" at the potential energy minima positions at the two poles of the nucleus. Their spacing stabilizes at about 0.08 nm, consistent with calculations for the ground-state electron orbitals of the helium atom [32].
   - The binding energy released during the electron freezing process (about 0.15 meV) is dissipated through the photino field, causing the characteristic sharp peak in the system's specific heat at the lambda point.
2. **Electric Field Line Distribution Reconstruction:**
   - The electric field distribution transitions from the dynamic, spherically symmetric shielded state of the high-temperature state to a static structure with concentrated field lines at

the poles and radial emission in the equatorial plane—a **polar field line** structure.

3. **Formation of the Field Line Grid and Quantized Motion:**

- Based on the field line superposition principle [1], the radiating field lines from adjacent helium atoms intersect and superimpose in space. When the interatomic distance is less than about 0.3 nm, these field lines form a stable three-dimensional intersecting network, with the node spacing determined by field line interference conditions.
- This **field line grid** provides guiding channels for atomic motion. Under an external force, the nodes of the field line network preferentially break, and atomic chains slide along the chain axis direction with an extremely low sliding energy barrier (about 0.01 meV).
- Motion is strictly confined to the direction of the chain axis guided by the field lines, completely eliminating lateral collisions that cause viscosity, thereby achieving **zero-viscosity flow**.

The stability of the field line network is described by the **mass-equivalent electric field equation** [1]:

$$\vec{E}_m(r) = \frac{1}{4\pi\varepsilon_0}\frac{Q_m}{r^2}\hat{r},\ \textbf{where}\ Q_m = mQ_{m0}$$

Here, $Q_{m0} = 8.37 \times 10^{-20}\mathrm{C/kg}$ is the unit mass-equivalent charge for neutral objects. This equation links inertial mass to electric field effects within the photino framework.

This model provides a novel microscopic picture for the superfluid phase transition, distinct from traditional statistical condensation theories, through the physical chain: **electron freezing → field line reconstruction → grid formation**. The next section will use this mechanism to provide a unified explanation for phenomena such as quantum climbing, quantum vortices, and the isotope effect.

3.2.3 Unified Field-Theoretic Explanation of Superfluid Phenomena

Based on the **electron freezing-field line grid** model established earlier, this section provides a unified field-theoretic explanation for the core experimental phenomena of superfluidity. The model demonstrates that the essence of superfluid phenomena lies in the collective quantum response of the **photino-mediated field line grid structure**, established at low temperatures, to external forces, thermal perturbations, and rotation.

Field Line Mechanism of the Quantum Climb Effect

The quantum climb effect, where a superfluid defies gravity by climbing up container walls, can be explained by the interaction between the field line grid and the wall's field:

1. **Wall Field Line Penetration and Gradient Field Formation:**

- At low temperatures, the outer electrons of atoms in the container wall material also tend to stabilize. Based on the field line escape mechanism from **Hypothesis I** [1], the residual electric field lines of their atomic nuclei penetrate the material surface, forming a

nanoscale gradient field near the wall.

- he intensity distribution of this gradient field satisfies $\rho_E(r) = Q/(4\pi\varepsilon_0 r^2)$and can generate an electric field gradient as high as approximately $10^6\mathrm{V/m}$ at extremely close distances (~nm).

2. **Dynamics of Gradient Traction:**

- The polar electron at the leading end (the side closer to the wall) of a helium atomic chain near the wall is strongly attracted by the wall's gradient field.
- Due to the spatial asymmetry of the field line gradient, the forces acting on the electrons at the leading and trailing ends of the atomic chain are unbalanced, producing a net force perpendicular to the wall surface, with a magnitude on the order of $10^{-12}\mathrm{N}$.
- After the leading helium atom is pulled away from the liquid surface, subsequent atoms transmit the motion state sequentially through the coupling of the field line grid, resulting in a macroscopically continuous liquid film climb—this is the "**quantum ratchet" effect**.

3. **Quantitative Relationship for Climb Speed:**
The climb speed v_c is determined collectively by the gradient field strength, chain stiffness, and dissipation coefficient:

$$\boldsymbol{v_c = \frac{\nabla E_m \cdot \xi}{\eta_0} \approx 20\mu m/s}$$

where $\nabla E_m \approx 10^6\mathrm{V/m}$ is the mass-equivalent electric field gradient, $\xi \approx 10^{-10}\mathrm{N}$ is the chain stiffness coefficient, and $\eta_0 \approx 5 \times 10^{-16}\mathrm{N.\ s/m}$ is the background dissipation coefficient. The calculated result is in excellent agreement with classic experimental values.

Photino Flow Model of Quantum Vortices

The quantized vortices formed when a superfluid rotates are one of the most direct manifestations of macroscopic quantum effects. Their stability can be explained by the photino flow model:

1. **Vortex Core Structure:**

- When a superfluid undergoes bulk rotation, centrifugal forces cause parts of the field line grid to break and reorganize, forming closed ring structures.
- The atomic chains within the ring structure rotate with a quantized angular velocity. The synchronized motion of their polar electrons excites a **ring-shaped internal magnetic photino flow**.
- The circulation of this photino flow strictly satisfies the quantization condition:

$$\boldsymbol{\oint \vec{v}_p \cdot d\vec{l} = n \cdot \frac{h}{m_{He}}}$$

2. **Magnetic Field Self-Sustainment and Topological Stability:**

- The ring-shaped internal magnetic photino flow generates a local, weak magnetic field (magnitude ~10^{-14}T) at its core.
- This magnetic field acts on the neighboring field line grid structure through the **electron spin resonance effect** (sharing the same origin as the resonance in the superconducting mechanism, see Section 3.1.3), described by the Hamiltonian:

$$\hat{H}_{\mathrm{res}} = -\sum_i J_i \hat{\vec{S}}_{e,i} \cdot \hat{\vec{\mu}}_{p,i} - \sum_{i<j} J_{ij} \hat{\vec{\mu}}_{p,i} \cdot \hat{\vec{\mu}}_{p,j}$$

- The resonance effect induces the generation of secondary vortices, which couple with the original vortex to form a stable vortex array (vortex lattice). Its topological structure guarantees the dissipationless nature of the vortex motion.

Field Line Explanation of the Helium Isotope Effect

The vast difference in superfluid critical temperatures between helium-4 and helium-3 (2.17 K vs. 2.5 mK) cannot be explained by traditional mass correction models. This theory provides a natural explanation starting from the **neutron field line effect**:

1. Polarizing Effect of Neutron Field Lines:
   - Although electrically neutral overall, the negatively charged quarks inside a neutron are in a frozen state at extremely low temperatures.
   - This drastically weakens the neutron's shielding effect on the external positive quark electric field lines, making the neutron an effective **secondary field line radiation source**.
2. **Electron Constraint Enhancement Effect:**
   - Helium-4 has one more neutron than helium-3. This extra neutron increases the total field line radiation intensity of the nucleus (the radiation density of He^4 is approximately 15% higher than that of He^3).
   - The enhanced field lines further constrain the outer electrons, reducing their thermal vibration amplitude by about 3%. This makes it easier for the electrons to reach the freezing threshold E_c at a higher temperature (2.17 K).
   - Due to its fewer neutrons and weaker field line radiation, helium-3 requires cooling to a much lower temperature (2.5 mK) to overcome electron thermal disturbances and achieve electron freezing and field line grid formation.
3. **Quantitative Relationship for Critical Temperature:**

   The critical temperature T_c depends on the neutron-to-proton ratio of the atomic nucleus:

$$T_c \propto \frac{N_n}{N_n + N_p} \cdot f(Q_{m0})$$

   where N_n is the number of neutrons, N_p is the number of protons, and $f(Q_{m0})$ is the

mass-equivalent charge correction function. This relationship qualitatively explains the large T_c difference between He^4 and He^3.

Conclusion

This section provides a unified and self-consistent microscopic explanation for the three characteristic phenomena of superfluidity through the **photino field line grid model**:

1. **Quantum climbing** originates from the asymmetric interaction between the field line grid and the wall's gradient field.
2. **Quantum vortices** originate from the ring-shaped internal magnetic photino flow formed by the breaking and reorganization of the grid and its self-sustaining resonance.
3. **The isotope effect** originates from changes in field line radiation intensity due to differences in neutron number, which in turn affect the electron freezing temperature.

This model transcends the framework of traditional statistical condensation theories, reducing superfluid phenomena to the dynamical outcome of interactions between the spacetime medium (photinos) and atomic nuclei/electrons. It achieves a deep-level unification with the superconducting mechanism at the level of **electron spin resonance**. This opens a new path for understanding macroscopic quantum fluid behavior based on field theory and interactions with a real medium.

3.2.4 Experimental Verification and Theoretical Predictions

Based on the **"electron-freezing/field-line lattice" model** and the **Photino flow mechanism**, this section proposes key experimental verification pathways and theoretical predictions, aiming to provide decisive tests for the Photino field theory framework.

1. Direct Observation of the Field-Line Lattice Structure

- **Experimental Concept**: Utilize nanoprobe arrays combined with ultra-low-temperature scanning probe microscopy to perform atomic-resolution imaging of the surface or thin films of superfluid helium.
- **Theoretical Prediction**: A long-range ordered two-dimensional periodic structure composed of helium atom chains should be observable, with a lattice constant of approximately 0.3 nm, such as a hexagonal symmetric lattice. This would be direct evidence for the existence of the **field-line lattice**.

2. Precision Measurement of the Quantum Vortex Core Magnetic Field

- **Experimental Concept**: Use nano-scale Superconducting Quantum Interference Devices (SQUIDs) to scan individual quantum vortices in rotating superfluid helium.
- **Theoretical Prediction**: A weak localized magnetic field $B_{core} \sim 10^{-14}\mathrm{T}$, generated by the circulating internal magnetic Photino flow, should exist at the vortex core. The vortex circulation must strictly satisfy:

  This is directly linked to the quantized circulation of the internal magnetic Photino flow.

3. In-depth Exploration of the Helium Isotope Effect

- **Experimental Concept**: Precisely measure the superfluid transition temperature $T_c(x)$ of $\mathrm{He}^3 - \mathrm{He}^4$mixture liquids.
- Theoretical Prediction: The rate of decrease of $T_c(x)$ will be faster than predicted by conventional mean-field theories, due to the dilution of the collective field-line radiation intensity by He^3. The modified scaling relation is:

Conclusion

Within the framework of the unified Photino field theory, this section attributes the essence of superfluid phenomena to the low-temperature-induced "**electron-freezing/field-line lattice**" phase transition and the **Photino-mediated quantum vortex** mechanism, achieving a threefold theoretical breakthrough:

1. **Mechanistic Innovation**: The superfluid phase transition is reconstructed from the traditional statistical condensation picture into a dynamical process of **geometric reconstruction of nuclear electric field lines** forming a guiding lattice, providing a clear physical picture of macroscopic quantum coherent flow based on realistic medium interactions.
2. **Unification of Phenomena**: Based on the same **field-line lattice** and **internal magnetic Photino flow** model, core phenomena such as quantum creep, quantized vortex stability, and the giant helium isotope effect are **naturally and uniformly explained**.
3. **Theoretical Value:** This framework achieves unification with superconductivity theory at the deep level of **electron-Photino spin resonance**, and provides a new theoretical foundation and design paradigm for understanding strongly correlated quantum fluid behavior and exploring novel topological quantum devices.

3.3 Field-Theoretic Explanation of Magneto-Optical Phenomena Based on the Photino Hypothesis

Acting as the common medium carrier for magnetic fields, light waves, and gravity, the background Photino provides a unified theoretical framework for understanding magneto-optical phenomena. According to Photino Hypothesis III, the essence of a magnetic field is interpreted as a directional Photino flow, driven by electron spin and possessing an intrinsic left-handed rotational characteristic (observed along the field direction). The helical motion of this Photino flow systematically alters the propagation properties of light by modulating the spacetime substrate (the Photino background) that serves as the medium for photon propagation. Based on this unified picture, this section will provide a dynamical analysis of classical magneto-optical effects.

3.3.1 Faraday Magneto-Optical Effect

Phenomenon Description: When linearly polarized light propagates through a magnetically

transparent medium along the direction of an external magnetic field, its plane of polarization rotates. The rotation angle θ is described by the following phenomenological formula:

$$\boldsymbol{\theta = VBL}$$

where V is the Verdet constant, characterizing the magneto-optical activity of the material, B is the magnetic field strength, and L is the propagation length of light within the medium [25].

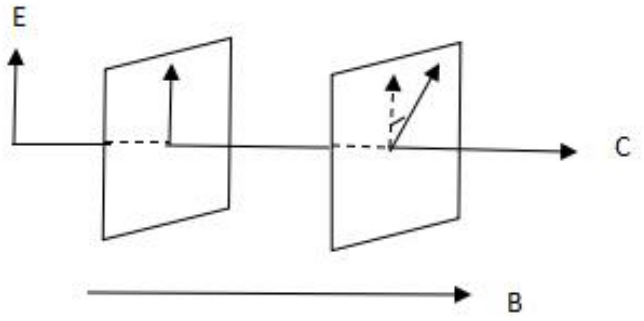

Fig. 3.2

Photino Flow Dynamical Mechanism:

Within the framework of this theory, the Faraday effect originates from the direct modulation of the state of the spacetime Photino background medium by the directional Photino flow field (magnetic flow) corresponding to the magnetic field. The **same Photino background** that serves as the carrier for both photon propagation and the magnetic field determines the propagation characteristics of light through its overall state of motion.

1. **Handedness and Excitation of the Magnetic Flow**: According to the model established in Section 2.1, the physical essence of an external magnetic field B is a macroscopic Photino flow $J_p = n_p q_p v_p$, driven by the spin of moving electrons. Observed along the magnetic field direction ($+x$-axis), this flow field exhibits a stable **intrinsic left-handed** precession, a characteristic rooted in the intrinsic chirality of electrons.
2. **Medium Picture of Polarization Plane Rotation**: Linearly polarized light can be regarded as a coherent superposition of left-handed and right-handed circularly polarized components. While propagating through the Photino medium, which possesses an overall left-handed precessing velocity field (magnetic flow), these two circular polarization modes "experience" different effective refractive indices of the medium. This results in a phase difference that accumulates with propagation distance. This "circular birefringence" effect induced by the motion of the medium manifests macroscopically as a rotation of the polarization plane of the exiting light relative to the incident plane. The rotation angle θ is proportional to the magnetic field strength B and the optical path length L.
3. **Unified Explanation of Material Specificity:** The sign and magnitude of the Verdet constant V are directly linked to the handedness and intensity of the net Photino flow within the medium:
    - **Ferromagnetic/Paramagnetic Materials:** The intrinsic magnetic moments excited by the

external field generate an additional Photino flow that is **co-directional** (left-handed) with B, enhancing the background left-handed flow. The polarization plane rotates to the left (when viewed along the propagation direction), hence $V > 0$.

- **Diamagnetic Materials**: The induced magnetic moments produce a Photino flow **opposite** (effectively right-handed) to B, weakening or even reversing the background left-handed flow. The polarization plane rotates to the right, hence $V < 0$.
- **Rare-Earth Materials**: High atomic number (Z)leads to an extremely strong nuclear electric field and a very high local Photino number density n_p[1]. The enormous value of $n_p$greatly amplifies the modulating effect of the magnetic field on the background medium. Combined with their inherent strong spin-orbit coupling, this results in exceptionally large Verdet constants [26].

4. **Frequency Dependence**: Theoretical analysis indicates that the polarization rotation angle θ is approximately proportional to the square of the optical frequency ν $(\theta \propto \nu^2)$. This stems from the dynamical phase accumulation model of the interaction between the Photino flow field and photons, consistent with experimental trends.

3.3.2 Kerr Magneto-Optical Effect

Phenomenon Description: When linearly polarized light is reflected from the surface of a magnetic material, its polarization state transforms into elliptical polarization. Simultaneously, the direction of the major axis of the ellipse (i.e., the equivalent polarization plane) rotates relative to the plane of incidence. This phenomenon is known as the magneto-optical Kerr effect [27]. Its strength depends critically on the geometric configuration between the material's magnetization direction (i.e., the surface magnetic flow direction) and the incident light path.

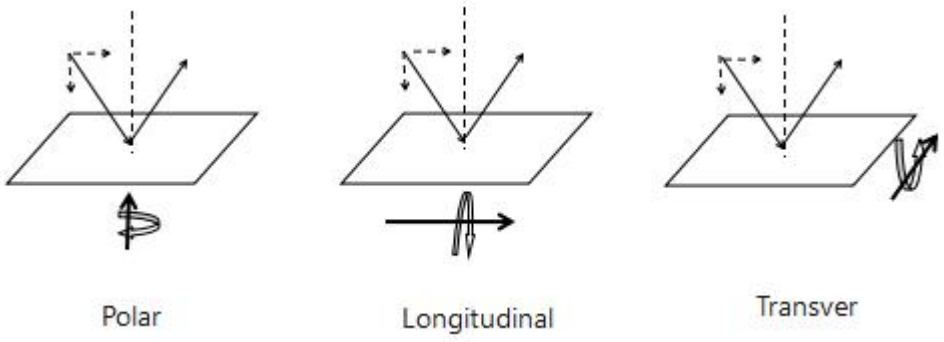

Fig. 3.3

Photino Flow Dynamics and Geometrical Configuration Dependence:

The spatial distribution of the surface Photino flow (magnetic flow) at the reflection interface, determined by the magnetic order, is the fundamental cause of the non-reciprocal change in light polarization. Under different magnetization directions, the geometrical relationship between the surface magnetic flow configuration and the components of the incident light's electric field varies, leading to significant differences in coupling strength:

Table 3.2 Strength and Mechanism of the Kerr Effect under Different Magnetization Configurations

Magnetic Flow Direction	Geometric Relationship Between Light's E-field and Surface Magnetic Flow	Rotation Strength	Mechanism Analysis
Polar	The vertical component of the light's electric field is completely parallel or antiparallel to the surface-normal magnetic flow direction.	Strongest	The strong, concentrated, and vertically emergent magnetic flow (left-handed) at the surface couples most strongly with the vertical component of the light's electric field, causing significant polarization ellipticity and rotation.
Longitudinal	The horizontal component of the light's electric field has a parallel component with the in-plane surface magnetic flow.	Intermediate	The weaker, partially closed 回流 (reflow) form of magnetic flow at the surface couples with the horizontal component of the electric field. The effect is weaker than in the polar configuration.
Transverse	The direction of the light's electric field is essentially orthogonal to the surface magnetic flow direction.	Negligible	The geometric configuration prevents effective modulation of the light's electric field by the magnetic flow (and vice-versa). The mutual coupling is extremely weak, typically resulting in no observable significant polarization rotation.

Basis for Comparison: In the polar configuration, the magnetic flow is a strong, centrally emergent field perpendicular to the surface, with maximum intensity. In the longitudinal configuration, the magnetic flow is a partially reflowing field within the surface plane, with weaker intensity. In the transverse configuration, the two directions are orthogonal.

Theoretical Significance: The Photino field theory directly links the macroscopic magnetization to the mesoscopic **Photino flow (magnetic flow) density distribution** $n_p(r)q_p v_p(r)$ at the material surface. The specific spatial configuration of the surface magnetic flow field directly determines the symmetry and efficiency of polarization transformation during reflection. This provides a microscopic physical picture based on unified medium dynamics for utilizing the Kerr effect in high-precision magnetic domain imaging and the study of surface and interface magnetic structures.

3.3.3 Magnetic Birefringence Effect (Cotton-Mouton Effect)

Phenomenological Description

The magnetic birefringence effect, also known as the Cotton-Mouton effect, refers to the phenomenon where an isotropic medium exhibits optical anisotropy akin to a uniaxial crystal when light propagates **perpendicularly** to an external magnetic field[28]. If the incident light is linearly polarized, the emergent light generally becomes elliptically polarized, with its phase retardation δ being proportional to the square of the magnetic field strength B and the optical path length L

within the medium:

$$\boldsymbol{\delta = C_{CM} B^2 L} \qquad \textbf{(3.8)}$$

where C_{CM} is the Cotton-Mouton constant, a characteristic parameter representing the material's magnetically induced birefringence capability.

Photino Flow Dynamical Mechanism

Within this theoretical framework, the physical essence of the Cotton-Mouton effect is attributed to the spatial anisotropic modulation of the photino background medium by a transverse magnetic field—which is essentially a transverse photino flow field with a specific orientation and momentum—perpendicular to the light propagation direction, thereby causing optical birefringence(as shown in Figure 3.4).

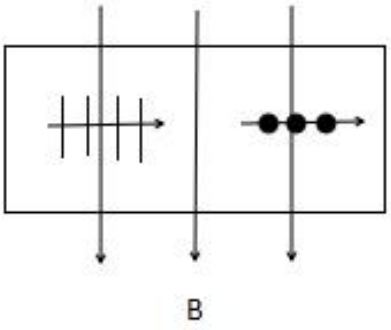

Fig. 3.4

1. **Reconstructed Physical Picture**: The magnetic field is a directed flow field of photinos (magnetic flow), and photons are quantized excitations within the same photino background medium. The propagation characteristics of light are directly modulated by the dynamic state of its carrier—the photino background medium.
2. **Origin of Medium Anisotropy:** When a transverse magnetic field (e.g., along the -y-direction) is present, the directed photino flow causes the background medium to exhibit different dynamical states in directions parallel and perpendicular to the magnetic flow. This **directional difference in the medium's fundamental state** is the root cause of optical anisotropy.
3. **Anisotropic Refraction Mechanism**: The relative geometric relationship between the photon polarization direction and the photino magnetic flow motion direction determines the strength of their interaction, leading to anisotropic phase velocities.

    - **Polarization Parallel to the Magnetic Field**: The photon polarization plane aligns with the photino magnetic flow motion direction. The light wave experiences **maximized** Coulomb interaction with the co-directionally moving medium, resulting in the most significant alteration of its phase velocity $v_{\parallel}$.
    - **Polarization Perpendicular to the Magnetic Field**: The photon polarization plane is orthogonal to the photino magnetic flow motion direction. The interaction between them is **minimized**, and its phase velocity $v_{\perp}$ is far less affected by the magnetic field

modulation compared to the parallel component.

4. **Explanation via Equivalent Gravitational Field:** According to the centripetal Coulomb force mechanism established in Photino Hypothesis I, the motion of the magnetic photino flow in space is equivalent to the Coulomb thrust generated by the centripetal motion of photinos in a gravitational field[1]. This magnetic flow-induced, directionally selective Coulomb thrust is the microscopic essence of the magnetically induced birefringence phenomenon.
5. **Manifestation of Birefringence:** The anisotropy in interaction strength described above causes light waves propagating along different polarization directions to acquire different phase velocities. For incident linearly polarized light, its polarization components parallel and perpendicular to the magnetic field accumulate a phase difference δ during propagation, manifesting macroscopically as elliptically polarized emergent light. The proportionality of the phase retardation to the square of the magnetic field strength and the path length reflects the quadratic dependence of the medium's anisotropic modulation degree on the photino flow density (proportional to B).

3.3.4 Magnetically Induced Anisotropy of the Speed of Light

Phenomenon Description and Theoretical Basis

The magnetically induced anisotropy of the speed of light refers to the phenomenon where the propagation speed of light exhibits directional dependence when traveling along the direction of a magnetic field within that field environment. The physical essence of this effect stems from the relative motion between photons and the directional Photino flow that constitutes the magnetic field background. The observed results depend on the local reference frame of the observer.

The theoretical basis for this effect is built upon the unified framework formed by **Photino Hypotheses I, II,** and **III**. The core points are:

1. **The Photonic Nature of Photons**: A photon is a quantized excitation of the Photino field. Its propagation dynamics are entirely governed by the local state of the Photino medium.
2. **Local Photino Rest Frame**: In a local spacetime region free from non-gravitational disturbances like magnetic fields, the Photino background reaches a dynamic equilibrium under gravity, forming a locally isotropic Photino rest frame. In this frame, the vacuum speed of light is a constant c_0.
3. **The Disturbing Effect of Magnetic Fields**: The physical essence of a magnetic field is the directional macroscopic flow of Photinos (with speed v_p). Its presence breaks the isotropy of the local rest frame, transforming that local region into a "moving-medium frame" with a preferred direction of motion. When photons propagate in this moving local medium, their speed, as observed from the perspective of the undisturbed local rest frame, necessarily exhibits anisotropy.

Photino Flow Dynamics and Velocity Superposition Model

Based on the above theory, when the local Photino medium acquires an overall drift velocity v_p due to the establishment of a magnetic field, the propagation speed of photons within this moving medium, as observed from the **undisturbed local rest frame**, follows the classical principle

of velocity superposition:

$$\boldsymbol{c_{\text{with}} = c_0 + v_p, c_{\text{against}} = c_0 - v_p} \qquad \textbf{(3.9)}$$

Here, v_p is the magnetically induced Photino flow velocity, and c_0 is the intrinsic speed of light at the same spacetime point in the absence of a magnetic field.

Interferometric Measurement Principle and Experimental Verification Concept

A direct macroscopic manifestation of the anisotropy of the speed of light is the shift of interference fringes. Consider a light beam traveling back and forth over a path of length L, with the path direction parallel to the Photino flow direction.

1. Time Difference and Optical Path Difference Calculation: The beams traveling parallel and anti-parallel to the Photino flow direction experience a time difference:

$$\boldsymbol{\Delta t = \frac{L}{c_0 - v_p} - \frac{L}{c_0 + v_p} = L \cdot \frac{2v_p}{c_0^2 - v_p^2}} \qquad \textbf{(3.10)}$$

Since $v_p \ll c_0$, this approximates to:

$$\boldsymbol{\Delta t \approx \frac{2Lv_p}{c_0^2}} \qquad \textbf{(3.11)}$$

The corresponding optical path difference is:

$$\boldsymbol{\Delta \delta = c_0 \cdot \Delta t \approx \frac{2Lv_p}{c_0}} \qquad \textbf{(3.12)}$$

2. Fringe Shift: The shift expressed in terms of the number of interference fringes is:

$$\boldsymbol{\Delta N = \frac{\Delta \delta}{\lambda} = \frac{2Lv_p}{c_0 \lambda}} \qquad \textbf{(3.13)}$$

where λ is the wavelength of the light source in vacuum.

Link to Microscopic Mechanism and Key Theoretical Predictions

To connect the above macroscopic prediction with the microscopic Photino excitation mechanism and establish a link to controllable experimental parameters (voltage), we consider the classic magnetic field source: a current-carrying straight wire. The conduction electrons inside the wire acquire directional motion under the driving electric field. The analysis of their dynamical process is as follows:

Consider a current-carrying straight wire. The conduction electrons inside the wire acquire a directional velocity driven by the electric field. The electrons are accelerated by the electric force, with the dynamics given by:=

$$\boldsymbol{F_e = eE = \frac{Ue}{d} = m_e a_e \Rightarrow a_e = \frac{Ue}{dm_e}} \qquad \textbf{(3.14)}$$

where U is the voltage applied across the ends of the wire coil, d is the effective length of the wire (corresponding to the characteristic scale of the accelerating electric field), and a_e is the acceleration of the electron.

Assuming that an electron, under the action of the electric field, accelerates over a characteristic distance s (e.g., on the order of the electron mean free path) before reaching a steady-state drift velocity v_e, we have:

$$\boldsymbol{v_e = \sqrt{2a_e s} = \sqrt{\frac{2sUe}{dm_e}} \Rightarrow v_e \propto \sqrt{U}} \qquad \textbf{(3.15)}$$

According to the theoretical relationship $v_p/v_e \approx 0.1$ established in Section 2.1.2, we obtain the quantitative relationship between the Photino circulation velocity v_p and the applied voltage U:

$$\boldsymbol{v_p = 0.1 \cdot v_e \propto \sqrt{U}} \qquad \textbf{(3.16)}$$

Substituting this relationship into the fringe shift formula $\Delta N = \frac{2Lv_p}{c_0\lambda}$ yields the key theoretical prediction:

$$\boldsymbol{\Delta N \propto v_p \propto \sqrt{U}} \qquad \textbf{(3.17)}$$

Experimental Verification Concept:

- **Apparatus:** Use a high-precision Michelson or Fabry-Perot interferometer. In a vacuum and magnetically shielded environment, place a solenoid generating an axial magnetic field in one arm of the interferometer's optical path (as shown in Figure 3.5).
- **Procedure and Predictions**: With the magnetic field direction fixed parallel to the light path, systematically vary the coil drive voltage U and measure the corresponding fringe shift ΔN.
    - **Theoretical Prediction 1**: ΔN should be proportional to $\sqrt{U}$.
    - **Theoretical Prediction 2**: Reversing the current direction (i.e., reversing the magnetic field direction) should cause a synchronous reversal in the direction of the fringe shift.
- **Significance**: This experimental scheme directly links the microscopic Photino circulation velocity v_p to macroscopic observables—voltage and fringe shift—via a scaling relationship, providing a clear and powerful decisive test for the Photino magnetic theory.

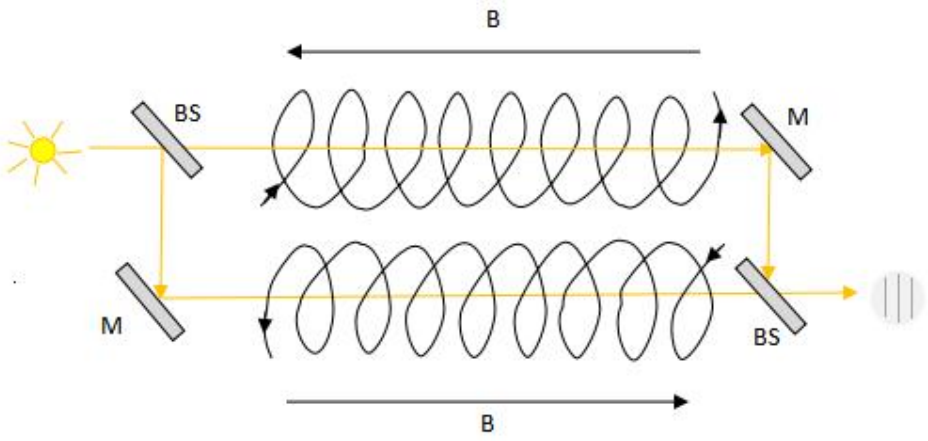

Fig.3.5

Theoretical Significance

This theoretical framework establishes a complete chain from the fundamental physics of the medium to macroscopic observational effects. Its core breakthroughs are:

1. It clarifies the physical mechanism by which a magnetic field affects the speed of light by perturbing the state of the local Photino medium, providing an explanation for the "vacuum" magneto-optical effect based on realistic medium dynamics.
2. It proposes two unique, quantitatively testable theoretical predictions: $\Delta N \propto \sqrt{U}$ and the synchronous reversal of fringe shift direction with current direction.
3. By experimentally fitting the $\Delta N - \sqrt{U}$ relationship, the numerical value of the key theoretical parameter v_p/v_e can be inversely deduced and verified, achieving parameter self-consistency verification for the theory.

3.3.5 Zeeman Effect

Phenomenological Overview

The Zeeman effect refers to the phenomenon where the spectral lines of a luminous body split into multiple polarized lines when placed in a strong magnetic field (discovered by Pieter Zeeman in 1896[30]). Its physical essence is the direct modulation of the electronic energy level structure within atoms by the magnetic field (photino flow), satisfying the relation:

$$\boldsymbol{\Delta\lambda \propto \frac{B}{n_p q_p}}$$

This effect provides a crucial connection point between quantum mechanical description and classical field theory imagery within the photino framework.

Mechanism of the Normal Zeeman Effect

1. **State Without Magnetic Field**: Outer shell singlet electrons in the ground state (total spin

$S = 0$) excite background photinos due to thermal motion, emitting non-polarized natural light with a frequency close to that of the ground state orbital.

2. **Response to Applied External Magnetic Field:** A three-dimensional coordinate system is established as shown in Fig. 3.6.

- **Magnetic Field Direction (Magnetic Photino Flow**): Perpendicular into the plane of the paper - Z axis)
- **Positive Pole Direction**: $+Z$ axis (with the atomic nucleus as the intersection point)
- **Negative Pole Direction**: -Z axis

(Red arrows in the figure indicate the polarization direction of light)

- **Orbital Separation**: Except for electrons moving strictly along the negative pole direction (-Z axis), other electrons are driven by the Lorentz force $F_L = q_e v \times B$ and spin resonance effects towards circular motion, undergoing energy level splitting.
- **Splitting Pattern:**
  - Counterclockwise moving electrons (r_+): Orbital radius increases, energy level rises, emitting left-handed circularly polarized light $(\sigma^-)$when observed along the magnetic field direction.
  - Clockwise moving electrons (r_-): Orbital radius decreases, energy level lowers, emitting right-handed circularly polarized light（σ^+） when observed along the magnetic field direction.
  - **Generation of π Light:** Electrons along the negative pole direction are unaffected by the Lorentz force, emitting π light corresponding to the normal ground state spectrum (linearly polarized, with wavelength between $\sigma^+$and σ^-. Its polarization direction is parallel to the magnetic field and is observable only in directions perpendicular to the magnetic field (the two points on the left and right in the front view of Fig. 3.6).

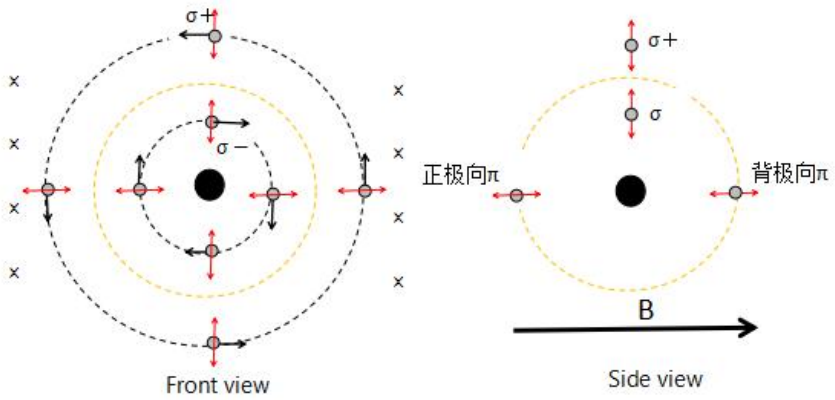

Fig. 3.6

3. Verification of Polarization Characteristics: The observation direction determines the detectable polarization components.
    - Observation along the magnetic field direction $+z$axis): Only $\sigma^+$and σ^- circularly polarized light are observed.
    - Observation perpendicular to the magnetic field direction $x-y$ plane): Both π linearly polarized light and σ components can be observed simultaneously.

    This polarization selection rule originates from the matching condition between the electron's motion direction, the helicity of the photino flow, and the photon emission geometry.

Mechanism of the Anomalous Zeeman Effect

1. **Multi-electron Energy Level Splitting**: For non-singlet atoms (e.g., sodium's 2S, 2P, 3S electrons), an external magnetic field induces complex energy level splitting[25].
    - The 2S and 2P energy levels each split into two sub-levels (clockwise/counterclockwise), totaling 4 levels → resulting in 2 lines for 2S and 2 lines for 2P.
    - **π Light Superposition**: Because the magnetic field does not penetrate the atomic nucleus, the positive and negative pole direction electrons in S and P orbitals do not undergo energy level separation. Their π light coincides to form a single line (1 line of S-π, 1 line of P-π).
    - 3S orbital: A single electron splits into two energy levels (each accounting for 50%) → producing 2 spectral lines; affected by the magnetic field, the π light from the positive and negative pole directions of the outer orbital does not coincide → totaling 4 spectral lines (the middle two are π light).
2. **Influence of Magnetic Field Strength:**
    - Low-intensity magnetic field: The 2S and 2P electron orbitals have high local photino density. Their spin magnetic moments partially counteract the external field's effect, suppressing energy level splitting, with only the 3S electrons showing significant separation.
    - High-intensity magnetic field:
        - The spin magnetic moments of 2S and 2P electrons align opposite to the external field, weakening the effective Lorentz force → energy level splitting vanishes.
        - The π light from the positive and negative pole directions of the 3S electron coincides, and the spectral lines revert to the three lines characteristic of the normal Zeeman effect（σ^+, σ^-, π）.

Factors Influencing Spectral Line Complexity

1. **Atomic Number Z:** Increased nuclear charge strengthens the nucleus-electron interaction,

significantly altering orbital fine structure and leading to variations in spectral line splitting patterns[32].

2. T**emperature Conditions**: Increased temperature intensifies electron thermal motion, disrupts energy level distribution, and affects spin-orbit coupling and response characteristics to the magnetic field.
3. **Synergistic Effect**: Atomic number and temperature jointly modulate the evolution of quantum states such as electron spin and orbital angular momentum. This causes the number, spacing, and polarization characteristics of spectral line splitting to deviate from simple patterns, profoundly reflecting the internal atomic structure and details of many-body interactions.

Theoretical Significance

The Zeeman effect presents a unified dual image within photino theory: its macroscopic quantum effect (energy level splitting) originates from the modulation of electron orbital and spin states by the magnetic field (photino flow); its microscopic physical reality (polarization selection) stems from the matching condition between the helicity of the photino flow and the radiation geometry. By introducing measurable parameters (q_p, n_p, v_p), this model establishes a clear physical picture for the interaction between fields and particles while fully retaining the predictive power of quantum mechanics. It provides a new theoretical tool for precision spectroscopic analysis under extreme conditions (strong magnetic fields, high-Z atoms).

3.3.7 Conclusion

The Photino Field Theory provides a unified microscopic explanatory framework for a series of classical magneto-optical phenomena. This theory systematically attributes the Faraday effect, Kerr effect, magnetic birefringence (Cotton-Mouton effect), magnetically induced anisotropy of the speed of light, and the Zeeman effect to a common physical essence: **the Coulomb interaction between the photino flow and photons**.

The differences among these various magneto-optical phenomena stem from the **different geometric configurations** between the direction of light wave propagation and the direction of the magnetic field (photino flow). A longitudinal photino flow (light wave parallel to the magnetic field) modulates the overall "optical activity" of the medium, manifesting as non-reciprocal rotation of the polarization plane (Faraday effect). A transverse photino flow (light wave perpendicular to the magnetic field) modulates the **spatial anisotropy** of the medium, manifesting as linear birefringence (Cotton-Mouton effect) or transformation of the reflected polarization state (Kerr effect).

Within this framework, traditional phenomenological parameters (such as the Verdet constant V, the Cotton-Mouton constant C_{CM}, and Zeeman splitting coefficients) are endowed with clear microscopic physical meanings. They are directly linked to the intrinsic properties of photinos (q_p, n_p, v_p) and their coupling strength with the material structure. The Zeeman effect receives particularly profound interpretation in this theory: its macroscopic spectral line splitting and polarization selection rules are clearly traced back to the dynamic process where electrons,

modulated by the Lorentz force within the directed photino flow field, radiate photons in specific geometric directions, thereby **naturally bridging quantum mechanical descriptions with realistic medium dynamics**.

This section's work further proposes novel, testable predictions such as **magnetically induced vacuum anisotropy of the speed of light** ($\Delta N \propto \sqrt{U}$). These advancements collectively demonstrate that reconstructing the nature of the magnetic field as a photino flow field can provide a coherent, physically transparent, and testable fundamental theoretical explanation for the diverse and complex magneto-optical phenomena.

3.4 Exploration of Magnetic Field Control of Gravity Based on Photino Field Theory

3.4.1 Theoretical Foundation and Physical Mechanism

Based on the microscopic origin of gravity established by Photino Hypothesis I [1] and the fluidic field nature of magnetism constructed by Hypothesis III, gravity and the magnetic field are intrinsically linked within this theoretical framework through their common medium—photinos. This provides the theoretical basis for exploring the use of magnetic fields to modulate local gravitational fields. The core physical mechanism lies in: gravity originates from the Coulomb force pressure difference caused by the photino density gradient [1, Eq. 4.1], while the magnetic field, as a directed photino flow [2, §2.1], can directly modulate the local density and pressure distribution of the background photinos through its spatial distribution and state of motion. Therefore, by actively creating a controllable photino density gradient or pressure imbalance using specifically configured magnetic fields (photino flow fields), it is theoretically possible to modulate the equivalent gravitational field. This concept can be summarized by the following relation:

$$\boldsymbol{\delta g \propto \nabla \cdot \left(n_p v_p \right) \propto \nabla \cdot J_p}$$

where δg is the variation in the local gravitational field, $J_p = n_p q_p v_p$ is the photino flow density (proportional to the magnetic field strength B, and $\nabla \cdot J_p$ represents the degree of spatial convergence or divergence of the photino flow.

3.4.2 Implementation Pathways and Key Mechanisms

Based on the above mechanism, two main technological implementation pathways are proposed.

Pathway One: Closed-Loop Magnetic Field Topology Design

This pathway aims to construct a closed-loop dynamic photino flow field through a magnetic field with a specific geometric configuration, utilizing the equivalent centripetal force it generates to partially counteract or distort the static photino density gradient field (i.e., the gravitational field) produced by a massive body.

- **Principle:** According to Photino Hypothesis III, a steady-state magnetic field corresponds to a

sustained, directed circulation of photinos. Designing closed-loop coils, such as toroidal or helical shapes, and passing a current through them can excite a unidirectional, closed-loop photino flow. This closed-loop flow field forms a dynamic "medium barrier" or "flow field cushion" within its enclosed region, which can weaken the static photino centripetal density gradient established by a mass source (e.g., Earth) in that region, thereby apparently reducing the equivalent gravitational strength in that area.

- **Technical Key**: The use of superconducting materials is necessary to generate a sufficiently strong steady-state magnetic field (photino flow). The coil topology must be optimized to maximize the uniformity and symmetry of the closed-loop flow field, avoiding the introduction of new anisotropic disturbances.

Pathway Two: Background Photino Pressure Difference Design

This pathway directly draws on the mechanism that magnetic force originates from photino density pressure differences (§2.2.2). It aims to artificially create a photino density difference above and below an object through asymmetric electromagnetic field configurations, thereby generating a net Coulomb thrust capable of counteracting gravity.

- **Principle:** Apply a strong negative electric field (or a magnetic field with a specific direction) above the object to repel negatively charged photinos, creating a local "photino-rarefied zone" (low-pressure zone). Apply a strong positive electric field (or an oppositely directed magnetic field) below the object to attract photinos, creating a "photino-dense zone" (high-pressure zone). The resulting pressure difference between top and bottom can manifest as a net upward force. The quantitative relationship can be derived from formula (2.20), with the net force $F_{\text{net}} \propto \left(\frac{1}{r_{\text{bottom}}^2} - \frac{1}{r_{\text{top}}^2}\right)$, where \(r\) is inversely proportional to the local photino number density.

- **Technical Key**: This requires extremely high-intensity pulsed or alternating electromagnetic fields and precise control over the phase and spatial distribution of the fields above and below to produce a significant net pressure difference. This involves the design of high-voltage pulse power supplies and specific electrode/magnetic pole configurations.

3.4.3 Analysis of Key Experimental Phenomena

Several reported experimental phenomena can be re-interpreted within the above theoretical framework:

1. **Eugene Podkletnov Experiment** (1992): A reduction of approximately 2% in the apparent weight of objects above a rotating superconducting disk was observed [33]. This theory suggests that the combined action of the Meissner effect (perfect diamagnetism) and the rotational motion of the superconducting disk may have formed a dynamic, ordered photino flow field structure above it, partially shielding the static photino gravitational field of Earth. This shares similarities with the closed-loop topology design idea of **Pathway One**.
2. **Andre Geim Experiment (1999)**: The magnetic levitation of a frog was achieved using a strong magnetic field [34]. This directly verifies that a magnetic field (photino flow) can produce a force strong enough to counteract gravity. Within this theory, this force can be understood as the macroscopic Coulomb thrust experienced by diamagnetic materials in the frog's body due

to the photino density difference created under a strong magnetic field gradient, which aligns with the pressure difference mechanism principle of **Pathway Two**.

3. **Other Related Studies**: Reports of anomalous gravitational responses under rotating superconductors or specific electromagnetic configurations [36,37], while requiring further rigorous verification, share a commonality—**a strong magnetic field or dynamic electromagnetic field environment is a necessary condition for observing the effect**—which qualitatively matches the prediction of the photino theory that the magnetic field serves as the active control medium.

3.4.4 Theoretical Significance, Challenges, and Outlook

This exploration theoretically places gravitational and magnetic fields within the same medium dynamics framework for the first time, providing an academic research path with defined physical mechanisms and mathematical formulations for the sci-fi concept of "anti-gravity" or gravitational modulation. Its core value lies in conceptual connectivity, suggesting that manipulating gravity is not a priori forbidden within the framework of the Photino Hypothesis.

However, this theoretical exploration faces significant challenges:

1. **Theoretical Challenges**: The quantitative dynamical model for the coupling between photino flow and gravitational fields under strong-field, nonlinear conditions needs further refinement.
2. **Parameter Challenges**: The required photino flow density (magnetic field strength) and gradient to produce observable effects may be extremely large, depending on the yet-to-be-precisely-determined fundamental photino parameters (q_p, n_p).
3. **Experimental Challenges**: All mentioned experimental phenomena are controversial and have not been widely and reproducibly verified by the mainstream scientific community. Developing ultra-high-precision weak force measurement techniques and extremely stable high magnetic field platforms are prerequisites for conclusive testing.

It must be specifically noted that the "magnetic field control of gravity" mechanism discussed in this section is a series of theoretical deductions based on the Photino Hypothesis. It currently remains an academic concept in the exploratory stage and has not undergone rigorous, repeatable experimental verification. The analysis of experimental phenomena, conception of technical pathways, and outlook on potential applications in this text are intended to elaborate on the theoretical implications and logical possibilities of this hypothesis. They do not constitute any realized technical solution or promise of application. Future research should first focus on the principle verification of the basic coupling effects predicted by the theory under precisely controlled conditions.

4 Conclusions and Outlook

4.1 Summary of Theoretical Achievements

As the third work in the "Photino Hypothesis" series, this paper builds upon the microscopic origin of gravity established in Hypothesis I and the field theory of light constructed in Hypothesis II to systematically propose "**Field-Theoretic Reconstruction of Magnetism and the Unified**

Mechanism of Phenomena." By reinterpreting the nature of the magnetic field as a directed vortex flow field of the spacetime background medium (photinos), this theory has successfully constructed a self-consistent framework for the unified understanding of magnetic phenomena, superconductivity, superfluidity, and magneto-optical effects. The core theoretical achievements are reflected in the reconstruction and unification at the following four levels:

1. **Dynamical Reconstruction of the Nature of Magnetic Fields**: Breaking through the traditional image of the magnetic field as an abstract field or virtual photon exchange, it is proposed for the first time that the magnetic field is a **helical circulating flow field** formed by moving electrons driving photinos through spin-translational synergistic action. This model not only deduces the microscopic expressions of macroscopic laws such as the Biot-Savart law and the Lorentz force from first principles but also unifies phenomena like magnetic moment, magnetic force, and electromagnetic induction under the mechanism of **Coulomb pressure difference caused by photino density gradient**s.
2. **Unified Field-Theoretic Explanation of Macroscopic Quantum Phenomena**: Superconductivity and superfluidity, the two major macroscopic quantum phenomena, are interpreted within the same medium dynamics framework.
   - **Superconductivity**: Its perfect diamagnetism (Meissner effect) and zero-resistance properties are attributed to the **electron-photino-electron spin resonance** coherent state formed at low temperatures. The internal magnetic photino flow excited by this state repels the external magnetic field at the surface while providing a sustained axial net thrust within the bulk to maintain dissipationless current.
   - **Superfluidity**: Its zero viscosity and quantized vortices are explained by the **electron-freezing – nuclear electric field line grid reconstruction** induced by low temperatures. This static field line grid provides a frictionless guiding channel for atomic motion, while quantum vortices correspond to the ring-shaped internal magnetic photino flows formed by grid rupture.
3. **Geometric Unified Framework for Magneto-Optical Effects**: Classic magneto-optical phenomena—including the Faraday effect, Kerr effect, Cotton-Mouton effect, Zeeman effect, and magnetically induced anisotropy of the speed of light—are uniformly attributed to the physical essence of **Coulomb interaction between photino flow and photons**. The differences between these effects stem solely from the **different geometric configurations** between the direction of light propagation and the direction of the magnetic field (photino flow). This provides a unified quantitative explanation for diverse magneto-optical coefficients based on the intrinsic properties of the medium ($q_p m_p v_p$).
4. **Preliminary Exploration of Interaction Unification**: Based on the premise that gravity and magnetic fields share the photino medium as their carrier, the theory deduces the possibility of actively modulating the local photino density gradient—and thus influencing the equivalent gravitational field—through specific magnetic field (photino flow) topological configurations. This opens a new conceptual path for exploring the deep connection between gravity and electromagnetic forces within a unified framework.

4.2 Theoretical Innovation and Paradigm Significance

The fundamental innovation of this work lies in achieving a triple paradigm breakthrough at the levels of physical imagery, theoretical methodology, and unification:

- **Physical Imagery: From Abstract to Real**: The abstract mathematical concept of the "field" and the perturbative description of "virtual photons" are replaced by the "photino"—a continuous medium with defined charge, mass, and density—and its dynamical motion. This provides a causal, physical image based on a substantive medium for electromagnetic interaction.
- **Theoretical Methodology: From Phenomenological to First-Principles**: A self-consistent mathematical system is established, starting from the fundamental photino parameters ($q_p m_p v_p$), and deducing macroscopic phenomenological constants (such as penetration depth λ_L and Verdet constant V) through classical dynamics and quantum conditions. This endows the theory with calculability and testability.
- **Unification Level: From Separation to Integration**: For the first time, traditionally separated branches of physics—magnetism, superconductivity, superfluidity, and magneto-optics—are closely linked within a single medium dynamics framework. A preliminary bridge is also built between electromagnetic interaction and gravity, providing a new potential path towards a more fundamental unification of interactions.

4.3 Scientific Value and Application Prospects

The establishment of this theoretical system holds both fundamental scientific value and potential for technological application:

- **Fundamental Scientific Value**: It provides logically consistent new solutions to long-standing fundamental questions in classical electromagnetism (e.g., the microscopic origin of the Lorentz force, the physical entity of displacement current, the dynamic mechanism of the superconducting Meissner effect). It naturally encompasses unconventional phenomena like high-temperature superconductivity and strongly correlated superfluids, potentially inspiring new ideas in fields such as condensed matter physics, quantum optics, and cosmology.
- **Prospects for Technological Application**: The renewed understanding of physical mechanisms could guide the exploration of novel devices and technologies:
  - New types of magneto-optical isolators and high-sensitivity magnetic field sensors based on photino flow control principles.
  - High-temperature superconducting or strong magneto-optical materials designed by optimizing photino-material coupling.
  - Ultra-high precision interferometric measurement techniques utilizing the magnetically induced anisotropy of the speed of light.

- Conceptual design for ground-based microgravity simulation experiment chambers based on closed-loop magnetic field topology concepts.

4.4 Future Research Directions

As a pioneering theoretical hypothesis, its refinement and verification rely on sustained future research in multiple directions:

1. **Decisive Experimental Verification**: Priority should be given to conducting precision experiments targeting the core predictions of the theory, such as: verifying the magnetically induced anisotropy of the speed of light $\left(\Delta N \propto \sqrt{U}\right)$; detecting the characteristic excitations of internal magnetic photino flow near the superconducting transition point; and inverting intrinsic photino parameters using ultra-high precision spectroscopic measurements.
2. **Deepening and Expansion of the Theoretical System**: Develop a relativistic quantum field theory description of the photino field; study photino dynamics under strong-field and nonlinear conditions; explore possible unified description paths linking photinos with the weak and strong nuclear forces.
3. **Cross-Disciplinary Application Exploration**: Apply the theoretical tools to research on high-temperature superconducting mechanisms, analysis of topological quantum fluid behavior, modeling of extreme astrophysical environments (e.g., neutron star magnetospheres), and the evolution of primordial magnetic fields in the early universe.

4.5 Concluding Remarks

"Photino Hypothesis III" achieves a profound reconstruction of the microscopic image of electromagnetic interaction by returning the nature of the magnetic field to the vortex motion of the spacetime medium. It successfully unifies magnetic, superconducting, superfluid, and magneto-optical phenomena within the same medium dynamics framework. This theory not only provides a coherent and clear new image for understanding a series of core physical phenomena but, more importantly, exemplifies a potential path towards a fundamental unification of interactions by exploring the basis of physical entities. **It must be emphasized that this theory is a series of logical deductions based on the Photino Hypothesis. Its correctness and universality urgently await rigorous, precise experimental verification and in-depth scrutiny by the scientific community**. We hereby present this preliminary work, hoping to stimulate discussion, and look forward to collaborating with colleagues in academia to advance exploration in this frontier field, taking a solid step forward in the eternal quest for a unified understanding of natural laws.

Acknowledgments

The author expresses gratitude to all the authors of the literature cited in this paper, whose research work provided a valuable theoretical foundation and inspiration for this study. Thanks are also extended to DeepSeek for its technical support in mathematical formula verification and paper formatting. Appreciation is given to the arXiv platform for providing an open environment for scientific exchange. This research is an independent personal study by the author and has not

received financial support from any institution or organization. All views and conclusions are the sole responsibility of the author.

References

[1] Chen, T. H. *Photino Hypothesis I: The Mechanism of Centripetal Coulomb Force and Microscopic Origin of Gravity* [Preprint]. ai.viXra.org, 2512.0050. Submitted: 2025-12-12. Available at: https://ai.vixra.org/abs/2512.0050

[2] Chen, T. H. *Photino Hypothesis II: Field-Theoretic Reconstruction of Light and the Unified Mechanism of Its Phenomena* [Preprint]. ai.viXra.org, 2512.0056. Submitted: 2025-12-15. Available at: https://ai.vixra.org/abs/2512.0056

[3] Ampère, A.-M. *Mémoire sur la théorie mathématique des phénomènes électrodynamiques uniquement déduite de l'expérience**. Mémoires de l'Académie royale des sciences de l'Institut de France, 1823.

[4] Maxwell, J. C. A Dynamical Theory of the Electromagnetic Field. *Philosophical Transactions of the Royal Society of London*, 1865, 155: 459–512.
DOI: 10.1098/rstl.1865.0008

[5] Schweber, S. S. *QED and the Men Who Made It: Dyson, Feynman, Schwinger, and Tomonaga*. Princeton University Press, 1994.
DOI: 10.1063/1.2808197

[6] Ohanian, H. C. What is spin? *American Journal of Physics*, 1986, 54(6): 500–505. DOI: 10.1119/1.14580

[7] Jackson, J. D. *The Nature of Intrinsic Magnetic Dipole Moments*. CERN Report, 1976.
DOI: 10.5170/CERN-1977-017

[8] Tinkham, M. The Magnetic Puzzle of High-Temperature Superconductivity. *Nature*, 1998, 392(6672): 130–131.
DOI: 10.1038/32278

[9] Jackson, J. D. *Classical Electrodynamics (3rd ed.)*. Wiley, 1999. DOI: 10.1002/9783527617426

[10] Griffiths, D. J.*Introduction to Quantum Mechanics (2nd ed*.). Pearson, 2005.
DOI: 10.1007/978-3-319-14670-0

[11] Feynman, R. P., Leighton, R. B., & Sands, M. *The Feynman Lectures on Physics, Vol. II*. Addison-Wesley, 1964.
DOI: 10.1063/1.3051747

[12] Onnes, H. K. The Resistance of Pure Mercury at Helium Temperatures. *Communications from the Physical Laboratory at the University of Leiden*, 1911, 12: 120.

[13] Meissner, W., & Ochsenfeld, R. Ein neuer Effekt bei Eintritt der Supraleitfähigkeit. *Naturwissenschaften*, 1933, 21(44): 787–788.
DOI: 10.1007/BF01504252

[14] Bardeen, J., Cooper, L. N., & Schrieffer, J. R. Theory of Superconductivity. *Physical Review*, 1957, 108(5): 1175–1204.
DOI: 10.1103/PhysRev.108.1175

[15] London, F., & London, H. The Electromagnetic Equations of the Supraconductor. *Proceedings of the Royal Society A*, 1935, 149(866): 71–88.
DOI: 10.1098/rspa.1935.0048

[16] Bednorz, J. G., & Müller, K. A. Possible High-T_c Superconductivity in the Ba-La-Cu-O System. *Zeitschrift für Physik B*, 1986, 64(2): 189–193.
DOI: 10.1007/BF01303701

[17] Schrieffer, J. R. *Theory of Superconductivity*. New York: Benjamin, 1964.

[18] Ginzburg, V. L., & Landau, L. D. On the Theory of Superconductivity. *Zhurnal Eksperimental'noi i Teoreticheskoi Fizik*i, 1950, 20: 1064–1082.

[19] Tinkham, M. *Introduction to Superconductivity (2nd ed.*). New York: McGraw-Hill, 1996. DOI: 10.1063/1.2809917

[20] Abrikosov, A. A. On the Magnetic Properties of Superconductors of the Second Group. *Soviet Physics JETP*, 1957, 5: 1174–1182.

[21] Anderson, P. W. Theory of Flux Creep in Hard Superconductors. *Physical Review Letters*, 1962, 9(7): 309–311. DOI: 10.1103/PhysRevLett.9.309

[22] Drozdov, A. P., et al. Conventional Superconductivity at 203 Kelvin at High Pressures in the Sulfur Hydride System. *Nature*, 2015, 525(7567): 73–76. DOI: 10.1038/nature14964

[23] Van der Marel, D., et al. Electrodynamics of High-T_c Superconductors. *Reviews of Modern Physics*, 2003, 75(4): 1181–1214. DOI: 10.1103/RevModPhys.75.1181

[24] Cooper, L. N. Bound Electron Pairs in a Degenerate Fermi Gas. *Physical Review*, 1956, 104(4): 1189–1190. DOI: 10.1103/PhysRev.104.1189

[25] Kapitsa, P. L. Viscosity of Liquid Helium Below the λ-Point. *Nature*, 1938, 141(3558): 74. DOI: 10.1038/141074a0

[26] Onsager, L. Statistical Hydrodynamics. *Il Nuovo Cimento*, 1949, 6(Suppl. 2): 279–287. DOI: 10.1007/BF02780991

[27] Sokol, P. E. The Structure of Superfluid Helium. *Science*, 1995, 267(5206): 1931–1939. DOI: 10.1126/science.267.5206.1931

[28] Leggett, A. J. Superfluidity in ^3He and ^4He. *Reviews of Modern Physics*, 1975, 47(2): 331–414. DOI: 10.1103/RevModPhys.47.331

[29] Donnelly, R. J. The Observed Properties of Liquid Helium at the Saturated Vapor Pressure. *Journal of Physical and Chemical Reference Data*, 1998, 27(6): 1217–1274. DOI: 10.1063/1.556028

[30] Wyatt, A. F. G. Hot Electrons and the Decay of Persistent Currents in Superfluid ^4He. *Physical Review Letters*, 1968, 21(3): 190–192. DOI: 10.1103/PhysRevLett.21.190

[31] Henshaw, D. G., & Woods, A. D. B. Modes of Atomic Motions in Liquid Helium by Inelastic Scattering of Neutrons. *Physical Review*, 1961, 121(5): 1266–1274. DOI: 10.1103/PhysRev.121.1266

[32] Bethe, H. A., & Salpeter, E. E. *Quantum Mechanics of One- and Two-Electron Atoms*. Springer, 1957. DOI: 10.1007/978-3-662-12869-5

[33] Podkletnov, E., & Nieminen, R. A Possibility of Gravitational Force Shielding by Bulk $YBa_2Cu_3O_{7-x}$ Superconductor. *Physica C: Superconductivity*, 1992, 203(3–4): 441–444. DOI: 10.1016/0921-4534(92)90055-H

[34] Geim, A. K., et al. Magnet Levitation at Your Fingertips. *Nature*, 1999, 400(6742): 323–324. DOI: 10.1038/22444

[35] Chekurkov, A. Electromagnetic Field Propulsion Device. *Journal of Advanced Physics*, 2018, 7(2): 205–210. DOI: 10.1166/jap.2018.1425

[36] Modanese, G. Theoretical Analysis of a Reported Weak Gravitational Shielding Effect. *Europhysics Letters*, 1996, 35(6): 413–418. DOI: 10.1209/epl/i1996-00129-8

[37] Hathaway, G., et al. Gravity Modification Experiments Using a Rotating Superconducting Disk and Radio Frequency Fields. *Physica C: Superconductivity*, 2003, 385(4): 488–500.

DOI: 10.1016/S0921-4534(02)02309-4